arXiv:2110.08524v1 [physics.atom-ph] 16 Oct 2021

Fock-space perturbed relativistic coupled-cluster theory for electric dipole polarizability of one-valence atomic systems: Application to Al and In

Ravi Kumar,[1] D. Angom,[2,3] and B. K. Mani[1,*]

[1]*Department of Physics, Indian Institute of Technology, Hauz Khas, New Delhi 110016, India*
[2]*Department of Physics, Manipur University, Canchipur 795003, Manipur, India*
[3]*Physical Research Laboratory, Ahmedabad - 380009, Gujarat, India*

We have developed a Fock-space relativistic coupled-cluster theory based method for the calculation of electric dipole polarizability of one-valence atoms and ions. We employ this method to compute the ground-state and spin-orbit coupled excited state electric dipole polarizability of Al and In. To check the quality of many-electron wavefunctions, we also compute the excitation energies of some low-lying states of Al and In. The effects of Breit interaction and QED corrections from the Uehling potential and the self-energy are included to improve the accuracy of α further. Our recommended value of ground-state α for both atoms are in good agreement with the previous theoretical results. From our computations, we find that more than 65% of contributions come from the dipolar mixing of $3p(5p)$ with $3d(5d)$ and $4s(6s)$-electrons for Al(In). The largest Breit and QED contributions are found to be 1.3% and 0.6%, respectively.

I. INTRODUCTION

Group-13 elements are a promising candidates for accurate optical atomic clocks as they are offer low fractional frequency errors [1–5]. It is to be mentioned that, the recent experiments, Refs. [6, 7], on Al^+ optical atomic clock have achieved a low fractional frequency error of 9.4×10^{-19} [6, 7] which is, perhaps, the most accurate clock in existence today. The electric dipole polarizability, α, of an atom or ion is a key parameter in estimating the accuracy of an atomic clock. It is used to estimate the blackbody radiation (BBR) shift, one of the dominant environment induced frequency shifts, in the transition frequencies of atoms and ions due to ac Stark effect. Since the measurement of α for individual states is non-trivial [8], accurate values from precision theory calculations play a crucial role in the development of new frequency and time standards for atomic clocks. The other potential implications of α include, discrete symmetry violations in atoms and ions [9, 10], condensates of dilute atomic gases [11–13], high-harmonic generation and ultrafast processes [14–17], and the search for the variation in the fundamental constants [18, 19].

In this work, we have employed a Fock-space perturbed relativistic coupled-cluster (FS-PRCC) theory to compute the properties of one-valence atomic systems in the external perturbations. We employ this method to compute the α for the ground state, $^2P_{1/2}$, and the spin-orbit (SO)-splitted excited state, $^2P_{3/2}$, of Al and In. In the literature, α for $^2P_{1/2}$ and $^2P_{3/2}$ states of Al and In have been calculated using different methods [20–25], including the coupled-cluster based methods like ours. One common trend in the reported data is, however, a large variation in the α values. For example, for $^2P_{1/2}$ state of Al, there is a difference of $\approx$ 10% in the smallest [20] and the largest [25] reported α values. The same trend is also observed in the experimental values [26–29]. The recent experiment [27] reports $\approx$ 20% larger α than Ref. [26] for Al. It is to be emphasized that, unlike the closed-shell atomic systems, calculation of α for an open-shell system is a challenging task and requires the inclusion of *core-core*, *core-valence* and *valence-valence* electrons correlations to the highest level of accuracy. Moreover, the inclusion of correlation effects from Breit interaction and QED corrections and the large basis sets are essential to tune the accuracy further. The aim of the present work is to fill this gap. We aim to: develop a Fock-space relativistic coupled-cluster (FS-RCC) theory based method to accurately account for an external perturbation in the properties calculation of one-valence atomic systems; compute the accurate value of α for Al and In; and quantify the various electron correlation effects embedded in the α of Al and In.

To test the accuracy of the wavefunctions, we have calculated to excitation energies of few low-lying states of Al and In using RCC theory. RCC is one of the most powerful many-body theories for atomic structure calculations. It accounts for the electron correlation to all-orders of residual Coulomb interaction, and has been used to calculate a plethora of properties in atomic systems. The implementation of such a theory and a FORTRAN code for the properties calculations of closed-shell and one-valence atomic systems without external perturbation is reported in our previous work [30]. For the properties calculation in the presence of external perturbation, we had reported a perturbed relativistic coupled-cluster (PRCC) theory for closed-shell in the works [31, 32] and references therein. One of the key merits of PRCC is that it does not employ the sum-over-state [33, 34] approach to incorporate the effects of a perturbation. The summation over all the possible intermediate states is subsumed in the perturbed cluster operators. Due to important prospects associated with α, it has been computed using a variety of other many-body methods in the literature. The recent review article by Mitroy *et al.* [35] provides a summary of α for several atoms and ions computed using different methods. The other reference which we found very useful is the Schwerdtfeger's updated table of α for neutral atoms [36]. The table provides an exhaustive list of references on experimental and theoretical values of α for several neutral atoms.

The remaining part of the paper is organized into five sec-

* bkmani@physics.iitd.ac.in

tions. In Sec. II, we discussed the RCC and PRCC theories for one-valence atomic systems where we derive the PRCC equations and also discuss in detail the contributing diagrams to each terms. In Sec. III, we discuss the calculation of α using PRCC theory. Here, we provide some dominant diagrams contributing to α. The basis set convergence and other calculational details are discussed in Sec. IV of the paper. In Sec. V, we analyze and present our results of excitation energy and dipole polarizability. Unless stated otherwise, all the results and equations presented in this paper are in atomic units ($\hbar = m_e = e = 1/4\pi\epsilon_0 = 1$).

II. METHODOLOGY

A. One-valence RCC Theory

The many-electron ground state wavefunction of an one-valence atom or ion in the RCC theory is expressed as

$$|\Psi_v\rangle = e^{(T^{(0)}+S^{(0)})}\,|\Phi_v\rangle, \tag{1}$$

where $|\Phi_v\rangle$ is the one-valence Dirac-Fock (DF) reference state, and is obtained by adding an electron to the closed-shell reference state, $|\Phi_v\rangle = a_v^\dagger|\Phi_0\rangle$. The operators $T^{(0)}$ and $S^{(0)}$ are the coupled cluster (CC) operators which act within the Hilbert spaces of the closed-shell and open-shell systems, respectively. The ground state $|\Psi_v\rangle$ is the solution of the eigenvalue equation

$$H^{\rm DCB}|\Psi_v\rangle = E_v|\Psi_v\rangle, \tag{2}$$

where $H^{\rm DCB}$ is the Dirac-Coulomb-Breit no-virtual-pair Hamiltonian and E_v is the exact energy of the one-valence system. For an atom with N-electrons, $H^{\rm DCB}$ is

$$H^{\rm DCB} = \sum_{i=1}^{N}\left[c\boldsymbol{\alpha}_i\cdot\mathbf{p}_i + (\beta_i-1)c^2 - V_N(r_i)\right] + \sum_{i<j}\left[\frac{1}{r_{ij}} + g^{\rm B}(r_{ij})\right], \tag{3}$$

where $\boldsymbol{\alpha}$ and β are the Dirac matrices, and $V_N(r_i)$ is the nuclear potential. And, the last two terms, $1/r_{ij}$ and $g^{textB}(r_{ij})$, are the Coulomb and Breit interactions, respectively. The effects of the negative-energy continuum states are avoided by employing a kinetically balanced finite Gaussian basis [37, 38].

In the RCC theory, the single and double excitations incorporate most of the electron correlation effects and provide a good description of the properties. Therefore, we can approximate $T^{(0)} = T_1^{(0)} + T_2^{(0)}$ and $S^{(0)} = S_1^{(0)} + S_2^{(0)}$, which is referred to as the coupled-cluster with singles and doubles (CCSD) approximation. These operators in the second quantized notation are

$$T_1^{(0)} = \sum_{ap} t_a^p a_p^\dagger a_a, \quad \text{and} \quad T_2^{(0)} = \frac{1}{2!}\sum_{abpq} t_{ab}^{pq} a_p^\dagger a_q^\dagger a_b a_a, \tag{4a}$$

$$S_1^{(0)} = \sum_{p} s_v^p a_p^\dagger a_v, \quad \text{and} \quad S_2^{(0)} = \sum_{apq} s_{va}^{pq} a_p^\dagger a_q^\dagger a_a a_v. \tag{4b}$$

Here, the indices $ab\ldots$ and $pq\ldots$ represent the core and virtual orbitals, respectively. And, $t_{\ldots}^{\ldots}$ and $s_{\ldots}^{\ldots}$ are the cluster amplitudes of the T and S operators, respectively. These closed-shell and one-valence operators are obtained by solving a set of coupled nonlinear equations and details are discussed in our previous works [30, 39, 40]. In the Ref. [30], we have provided descriptions of the computational implementation of RCC theory for the properties calculations of the closed-shell and one-valence systems without an external perturbation.

B. One-valence PRCC theory

In the presence of an external perturbation, the wavefunction and the energy of the system are modified. For the electric dipole polarizability, the perturbation is due to the interaction between the external electric field $\mathbf{E}_{\rm ext}$ and the induced electric dipole moment of the system $\mathbf{D}$. And, the interaction Hamiltonian is $H_1 = -\mathbf{D}\cdot\mathbf{E}_{\rm ext}$. We refer the modified eigenstate as the perturbed eigenstate, $|\tilde{\Psi}_v\rangle$, and the modified energy as the perturbed energy, $\tilde{E}_v$. In the PRCC theory, $|\tilde{\Psi}_v\rangle$ is expressed as

$$|\tilde{\Psi}_v\rangle = e^{T^{(0)}}\left[1+\lambda\mathbf{T}^{(1)}\cdot\mathbf{E}_{\rm ext}\right]\left[1+S^{(0)}+\lambda\mathbf{S}^{(1)}\cdot\mathbf{E}_{\rm ext}\right]|\Phi_v\rangle, \tag{5}$$

where, λ is the perturbation parameter. The operators $\mathbf{T}^{(1)}$ and $\mathbf{S}^{(1)}$ are referred to as the perturbed closed-shell and one-valence cluster operators, respectively, and both are rank one operators. The operator $\mathbf{T}^{(1)}$ is obtained by solving a set of coupled perturbed equations within the Hilbert space of the occupied electrons. The details on its tensor representation and the PRCC equations are discussed in our previous works on the dipole polarizability of the closed-shell atomic systems [31, 41]. So, here, we discuss only the tensor representation and PRCC equations of the open shell cluster operator $\mathbf{S}^{(1)}$.

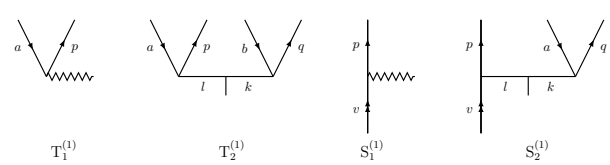

FIG. 1. Diagrammatic representations of $\mathbf{T}_1^{(1)}$, $\mathbf{T}_2^{(1)}$, $\mathbf{S}_1^{(1)}$ and $\mathbf{S}_2^{(1)}$ perturbed cluster operators.

Similar to the case of $T^{(0)}$ and $S^{(0)}$ operators, in the CCSD approximation, we take $\mathbf{S}^{(1)} = S_1^{(1)} + S_2^{(1)}$. And, these in the second quantized notations,

$$\mathbf{S}_1^{(1)} = \sum_{p} \xi_v^p \mathbf{C}_1(\hat{r}) a_p^\dagger a_v, \tag{6a}$$

$$\mathbf{S}_2^{(1)} = \sum_{apq}\sum_{lk} \xi_{va}^{pq}(l,k)\mathbf{C}_l(\hat{r}_1)\mathbf{C}_k(\hat{r}_2) a_p^\dagger a_q^\dagger a_a a_v. \tag{6b}$$

Here, $\xi_{\ldots}^{\ldots}$ represents the cluster amplitude for the operator $\mathbf{S}^{(1)}$. The one-body operator $\mathbf{S}_1^{(1)}$ is an odd parity opera-

tor and expressed in terms of a rank-one **C**-tensor. It satisfies the orbital-parity and orbital-triangular selection rules, $(-1)^{l_v+l_p} = -1$ and $|j_v - j_p| \leqslant 1 \leqslant (j_v + j_p)$, respectively. The tensor structure of the two-body operator $\mathbf{S}_2^{(1)}$ involves two **C**-tensors with ranks l and k associated with its two-vertices. These two **C**-tensors are coupled to give a rank-one operator, $\mathbf{S}_2^{(1)}$. The allowed orbital-parity and and orbital-triangular selections rules for $\mathbf{S}_2^{(1)}$ are, $(-1)^{l_v+l_p} = -(-1)^{l_a+l_q}$ and $|j_v - j_p| \leqslant l \leqslant (j_v + j_p)$, $|j_a - j_q| \leqslant k \leqslant (j_a + j_q)$, respectively. The diagrammatic representations of $\mathbf{T}^{(1)}$ and $\mathbf{S}^{(1)}$ are shown in the Fig.1.

In analogy with the Eq. (2), $|\tilde{\Psi}_v\rangle$ is the solution of the eigenvalue equation

$$\left(H^{\text{DCB}} + \lambda H_1\right)|\tilde{\Psi}_v\rangle = \tilde{E}_v|\tilde{\Psi}_v\rangle, \tag{7}$$

here, within the first-order time-independent perturbation theory, the perturbed energy $\tilde{E}_v \equiv E_v$ as the first-order correction vanishes due to the odd parity nature of H_1. Using Eq. (5) in the eigenvalue equation (7) and by operating with $e^{-T^{(0)}}$ from left, retaining the terms first order in λ, we get

$$\begin{aligned}&\left[e^{-T^{(0)}}H^{\text{DCB}}e^{T^{(0)}}\left(\mathbf{S}^{(1)}\cdot\mathbf{E}_{\text{ext}}\right) + e^{-T^{(0)}}H^{\text{DCB}}e^{T^{(0)}}\left(\mathbf{T}^{(1)}\cdot\mathbf{E}_{\text{ext}}\right)\left(1+S^{(0)}\right) + e^{-T^{(0)}}H_1e^{T^{(0)}}\left(1+S^{(0)}\right)\right]|\Phi_v\rangle \\ &= \left[E_v\left(\mathbf{S}^{(1)}\cdot\mathbf{E}_{\text{ext}}\right) + E_v\left(\mathbf{T}^{(1)}\cdot\mathbf{E}_{\text{ext}}\right)\left(1+S^{(0)}\right)\right]|\Phi_v\rangle.\end{aligned} \tag{8}$$

Using the definition of the normal ordered Hamiltonian, $H_N = H^{\text{DCB}} - \langle\Phi_v|H^{\text{DCB}}|\Phi_v\rangle$, and dropping E_{ext} for simplicity from both sides of the equation, we can write

$$\begin{aligned}&\left[\bar{H}_N\mathbf{S}^{(1)} + \bar{H}_N\mathbf{T}^{(1)}\left(1+S^{(0)}\right) + \bar{H}_1(1+S^{(0)})\right]|\Phi_v\rangle = \\ &\Delta E_v\left[\mathbf{S}^{(1)} + \mathbf{T}^{(1)}\left(1+S^{(0)}\right)\right]|\Phi_v\rangle\end{aligned} \tag{9}$$

where, $\Delta E_v, = E_v - \langle\Phi_v|H^{\text{DCB}}|\Phi_v\rangle$ is the correlation energy of one-valence atom. And, $\bar{H}_N, = e^{-T^{(0)}}H_Ne^{T^{(0)}}$, is a similarity transformed Hamiltonian. Using the Wick's theorem, it can be reduced to

$$\begin{aligned}\bar{H}_N = H_N &+ \{\overbracket{H_NT^{(0)}}\} + \frac{1}{2!}\{\overbracket{\overbracket{H_NT^{(0)}}T^{(0)}}\} \\ &+ \frac{1}{3!}\{\overbracket{\overbracket{\overbracket{H_NT^{(0)}}T^{(0)}}T^{(0)}}\} + \frac{1}{4!}\{\overbracket{\overbracket{\overbracket{\overbracket{H_NT^{(0)}}T^{(0)}}T^{(0)}}T^{(0)}}\}\end{aligned} \tag{10}$$

By projecting Eq. (9) with singly and doubly-excited determinants, $\langle\Phi_v^p|$ and $\langle\Phi_{va}^{pq}|$, respectively, and using the Wicks's theorem to remove the disconnected terms, we obtain the PRCC coupled equations for singles and doubles as

$$\langle\Phi_v^p|\bar{H}_1 + \{\overbracket{\bar{H}_1S^{(0)}}\} + \{\overbracket{\overbracket{\bar{H}_N\mathbf{T}^{(1)}}(1+S^{(0)})}\} + \{\overbracket{\bar{H}_N\mathbf{S}^{(1)}}\}\Phi_v\rangle = E_v^{\text{att}}\langle\Phi_v^p|\mathbf{S}_1^{(1)}|\Phi_v\rangle, \tag{11a}$$

$$\langle\Phi_{va}^{pq}|\bar{H}_1 + \{\overbracket{\bar{H}_1S^{(0)}}\} + \{\overbracket{\overbracket{\bar{H}_N\mathbf{T}^{(1)}}(1+S^{(0)})}\} + \{\overbracket{\bar{H}_N\mathbf{S}^{(1)}}\}\Phi_v\rangle = E_v^{\text{att}}\langle\Phi_{va}^{pq}|\mathbf{S}_2^{(1)}|\Phi_v\rangle. \tag{11b}$$

Here, E_v^{att} is the attachment energy of the valence electron and is expressed as $E_v^{\text{att}} = \epsilon_v + \Delta E_v$, where ϵ_v is the single-particle energy. In deriving these equations we have used the relations, $\langle\Phi_v^*|\mathbf{T}^{(1)}|\Phi_v\rangle = 0$ and $\langle\Phi_v^*|\mathbf{T}^{(1)}S^{(0)}|\Phi_v\rangle = 0$, as they do not contribute, where $*$ represents the single and doubly excited determinant. We solve these coupled nonlinear equations using the Jacobi method. To remedy the slow convergence of this method we employ direct inversion of the iterated subspace (DIIS) [42].

C. Linearized PRCC

The Eqs. (11a) and (11b) contain all the CC terms associated with the PRCC equations of the one-valence system. And, therefore, provides an accurate description of the properties of the system. However, solving these equations is computationally expensive due to the large number of many-body diagrams arising from the contractions with multiple CC operators. One simple approach to mitigate this is to retain terms which are linear in the CC operators. And, this also provides reliable results as in most of the cases the contribution from the nonlinear terms is small. So, retaining the terms linear in CC operators, we can write Eqs. (11a) and (11b) as

$$\begin{aligned}&\langle\Phi_v^p|H_1 + \{\overbracket{H_1T^{(0)}}\} + \{\overbracket{H_1S^{(0)}}\} + \{\overbracket{H_N\mathbf{T}^{(1)}}\} \\ &+\{\overbracket{H_N\mathbf{S}^{(1)}}\}\Phi_v\rangle = E_v^{\text{att}}\langle\Phi_v^p|\mathbf{S}_1^{(1)}|\Phi_v\rangle,\end{aligned} \tag{12a}$$

$$\begin{aligned}&\langle\Phi_{va}^{pq}|H_1 + \{\overbracket{H_1T^{(0)}}\} + \{\overbracket{H_1S^{(0)}}\} + \{\overbracket{H_N\mathbf{T}^{(1)}}\} \\ &+\{\overbracket{H_N\mathbf{S}^{(1)}}\}\Phi_v\rangle = E_v^{\text{att}}\langle\Phi_{va}^{pq}|\mathbf{S}_2^{(1)}|\Phi_v\rangle.\end{aligned} \tag{12b}$$

We refer to these equations as the linearized perturbed coupled-cluster (LPRCC) equations. The LPRCC incorpo-

rates all the important many-body effects like random-phase approximation and provides a good description of the one-valence atomic or ionic properties in the presence of perturbation.

D. PRCC diagrams

To solve the coupled-cluster amplitude Eqs.(11a) and (11b), we have to evaluate all the possible terms arising from each of the matrix elements in the equations. There are several terms and the book keeping is simplified with the many-body Goldstone diagrammatic approach. In this section we describe the Goldstone diagrams arising from the matrix elements and these are evaluated manually. It is, however, possible to identify diagrams computationally as well [43]. We have adopted the manual approach for the convenience in evaluating the angular factors. For simplicity, from here onwards, as it should be the case for α, we use $\mathbf{D}$ in place of H_1.

1. $\bar{\mathbf{D}}$

For the one-valence system, from the definition of the similarity transformed Hamiltonian in Eq. (10), using the CSSD approximation we get

$$\bar{\mathbf{D}} = \mathbf{D} + \overline{\mathbf{D}T_1^{(0)}} + \overline{\mathbf{D}T_2^{(0)}}. \tag{13}$$

The terms with two or higher orders of $T^{(0)}$ do not contribute to the PRCC equation for one-valence system. The first term, $\mathbf{D}$, is the bare dipole operator and contributes to the equation of $\mathbf{S}_1^{(1)}$. The two remaining terms represent the contraction with the unperturbed operator $T^{(0)}$ and contribute to the PRCC equations of the $\mathbf{S}_1^{(1)}$ and $\mathbf{S}_2^{(1)}$, respectively. In total, there are 3 diagrams from $\bar{\mathbf{D}}$, and these are shown in Fig. 2. Using the algebra of evaluating the Goldstone diagrams [44], we can write the algebraic expressions of the diagrams as

$$\langle \mathbf{D} \rangle_v^p + \langle \overline{\mathbf{D}T^{(0)}} \rangle_v^p = \mathbf{r}_{pv} - \sum_a \mathbf{r}_{av} t_a^p, \tag{14a}$$

$$\langle \overline{\mathbf{D}T^{(0)}} \rangle_{va}^{pq} = -\sum_b \mathbf{r}_{bv} t_{ab}^{qp}, \tag{14b}$$

respectively. Here, in atomic units $\mathbf{D} \equiv -\mathbf{r}$ and $\mathbf{r}_{ij} = \langle i|\mathbf{r}|j\rangle$ is the electronic part of the single-particle matrix element of the dipole operator. And, $\langle \cdots \rangle_v^p$ and $\langle \cdots \rangle_{vb}^{pq}$ represent the matrix elements $\langle \Phi_v^p| \cdots |\Phi_v\rangle$ and $\langle \Phi_{va}^{pq}| \cdots |\Phi_v\rangle$, respectively.

2. $\bar{\mathbf{D}}S^{(0)}$

Like the first term, consider the second term in Eqs.(11a) and (11b). Expanding the similarity transformed operator $\bar{\mathbf{D}}$ in terms of $T^{(0)}$, we can write

$$\overline{\mathbf{D}S^{(0)}} = \overline{\mathbf{D}S_1^{(0)}} + \overline{\mathbf{D}S_2^{(0)}} + \overline{\mathbf{D}T_1^{(0)}S_1^{(0)}} + \overline{\mathbf{D}T_2^{(0)}S_1^{(0)}} + \overline{\mathbf{D}T_1^{(0)}S_2^{(0)}}. \tag{15}$$

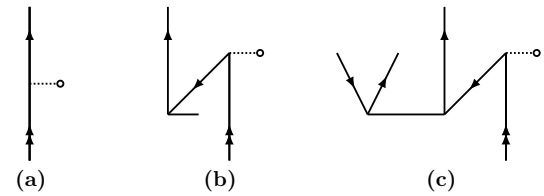

FIG. 2. Single and double PRCC diagrams contributing to the term $\bar{\mathbf{D}}$ of Eqs. (11a) and (11b), respectively.

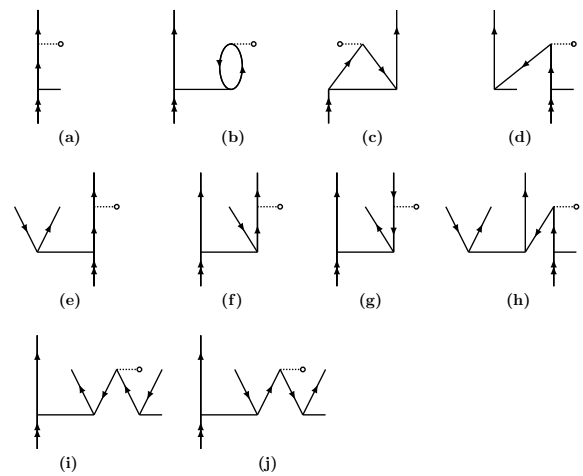

FIG. 3. Single and double PRCC diagrams contributing to the term $\overline{\mathbf{D}S^{(0)}}$ of PRCC Eqs. (11a) and (11b), respectively.

The terms having higher than two orders of CC operators do not contribute. The first three terms in the above equation contribute to the PRCC equation of $\mathbf{S}_1^{(1)}$ and leads to 4 diagrams. The diagrams are shown in Fig. 3(a-d). Except for the first term, all the other terms contribute to the PRCC equation of $\mathbf{S}_2^{(1)}$. In total there are 6 diagrams from these terms and these are shown in Fig. 3(e-j). The corresponding algebraic expressions are

$$\langle \overline{\mathbf{D}S^{(0)}} \rangle_v^p + \langle \overline{\mathbf{D}T^{(0)}S^{(0)}} \rangle_v^p = \sum_q \mathbf{r}_{pq} s_v^q + \sum_{aq} \mathbf{r}_{aq} (s_{va}^{pq} - s_{va}^{qp} - t_a^p s_v^q), \tag{16a}$$

$$\langle \overline{\mathbf{D}S^{(0)}} \rangle_{va}^{pq} + \langle \overline{\mathbf{D}T^{(0)}S^{(0)}} \rangle_{va}^{pq} = \sum_r (\mathbf{r}_{pr} s_{av}^{qr} + \mathbf{r}_{qr} s_{va}^{pr}) - \sum_b \mathbf{r}_{ba} s_{vb}^{pq} - \sum_{br} \mathbf{r}_{br} (t_{ab}^{qp} s_v^r + t_a^r s_{vb}^{pq} + t_b^q s_{va}^{pr}). \tag{16b}$$

This term is an important one in PRCC theory as it subsumes the many-body effects of the core-polarization.

3. $\bar{H}_N \mathbf{T}^{(1)}$

Unlike the previous two terms where the dipole operator appears explicitly, in this term, the effects of the perturbation is embedded in a rank one operator, $\mathbf{T}^{(1)}$. We can expand this

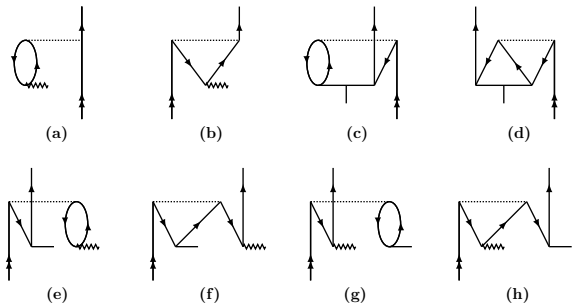

FIG. 4. Single PRCC diagrams contributing to the term $\overline{\bar{H}_N\mathbf{T}^{(1)}}$ of Eq. (11a).

as

$$\overline{\bar{H}_N\mathbf{T}^{(1)}} = \overline{H_N\mathbf{T}^{(1)}}+\overline{\overline{H_N T^{(0)}}\mathbf{T}^{(1)}}+\frac{1}{2}\overline{\overline{\overline{H_N T^{(0)}}T^{(0)}}\mathbf{T}^{(1)}} \quad (17)$$

Consider first the PRCC equation of the $\mathbf{S}_1^{(1)}$. Only the first two terms contribute. The PRCC diagrams from these terms are obtained by invoking all the possible contractions between the H_N and CC operators. There are 8 diagrams and these are shown in Fig. 4. We do not consider the diagrams arising from the one-body part of H_N. These do not contribute as we use Dirac-Fock orbitals in our calculations. The algebraic expression of these diagrams are given in Eq.(18b). In the equation, g_{ijkl} represents the matrix element $\langle ij|1/r_{12} + g^B(r_{12})|kl\rangle$ and $\tilde{g}_{ijkl}, = (g_{ijkl} - g_{ijlk})$, is an antisymmetric matrix element.

In the PRCC equation of $\mathbf{S}_2^{(1)}$, all the terms contribute and leads to 29 diagrams. These diagrams are shown in Fig. 5. Like in the case of $\mathbf{S}^{(1)}$, we do not include the diagrams from the one-body part of the H_N. The algebraic expression of these diagrams are given in the Eq.(18b). In the equation we see the emergence of a trend. The number of terms in this equation far exceed those in $\mathbf{S}_1^{(1)}$. This trend is there in the remaining non-linear terms as well.

$$\langle\overline{H_N\mathbf{T}^{(1)}}\rangle_v^p + \langle\overline{\overline{H_N T^{(0)}}\mathbf{T}^{(1)}}\rangle_v^p = \sum_{aq}\tilde{g}_{apqv}\tau_a^q + \sum_{abq}\left[-\tilde{g}_{abqv}\tau_{ab}^{qp} + g_{abvq}\left(-t_a^p\tau_b^q + t_a^q\tau_b^p - t_b^q\tau_a^p + t_b^p\tau_a^q\right)\right] \quad (18a)$$

$$\begin{aligned}\langle\overline{H_N\mathbf{T}^{(1)}}\rangle_{va}^{pq} + \langle\overline{\overline{H_N T^{(0)}}\mathbf{T}^{(1)}}\rangle_{va}^{pq} + \langle\overline{\overline{\overline{H_N T^{(0)}}T^{(0)}}\mathbf{T}^{(1)}}\rangle_{va}^{pq} &= -\sum_b g_{bqva}\tau_b^p + \sum_{bc} g_{bcva}\tau_{bc}^{pq} - \sum_{br}\left[g_{bpvr}\tau_{ba}^{rq} + g_{bqvr}(\tau_{ba}^{pr}\right.\\ &\left.+ \tau_b^p t_a^r + t_b^p\tau_a^r)\right] + \sum_{bc} g_{bcva}(\tau_b^p t_c^q + t_b^q\tau_c^q) + \sum_{bcr} g_{bcvr}\left(-t_{ba}^{pq}\tau_c^r + t_{ab}^{qr}\tau_c^p + t_{ba}^{pr}\tau_c^q + t_{bc}^{pq}\tau_a^r + t_{ca}^{pq}\tau_b^r - t_{ca}^{rq}\tau_b^p + t_{ac}^{rq}\tau_b^p\right.\\ &\left.- \tau_{ba}^{pq}t_c^r + \tau_{ab}^{qr}t_c^p + \tau_{ba}^{pr}t_c^q + \tau_{bc}^{pq}t_a^r + \tau_{ca}^{pq}t_b^r - \tau_{ca}^{rq}t_b^p + \tau_{ac}^{rq}t_b^p + \tau_a^r t_b^p t_c^q + \tau_c^q t_b^p t_b^q + \tau_b^p t_a^r\right)\end{aligned} \quad (18b)$$

4. $\bar{H}_N\mathbf{T}^{(1)}S^{(0)}$

This term involves one each of the perturbed and unperturbed CC operators $\mathbf{T}^{(1)}$ and $S^{(0)}$, respectively. And, the term contributes to the nonlinear PRCC equation. By expanding $\bar{H}_N$, we obtain

$$\overline{\overline{\bar{H}_N\mathbf{T}^{(1)}}S^{(0)}} = \overline{\overline{H_N\mathbf{T}^{(1)}}S^{(0)}} + \overline{\overline{\overline{H_N T^{(0)}}\mathbf{T}^{(1)}}S^{(0)}}. \quad (19)$$

The higher order terms will not contribute. As to be expected, several diagrams arise from this term due to various possible contractions between $H_{\rm N}$ and CC operators. For the PRCC equation of $\mathbf{S}_1^{(1)}$, there are 14 diagrams from this term. And, these are are shown in the left panel of Fig. 6. The algebraic expressions of these diagrams are given in Eq.(20).

$$\begin{aligned}\langle\overline{\overline{H_N\mathbf{T}^{(1)}}S^{(0)}}\rangle_v^p + \langle\overline{\overline{\overline{H_N T^{(0)}}\mathbf{T}^{(1)}}S^{(0)}}\rangle_v^p &= \sum_{aqr} g_{apqr}(\tau_a^q s_v^r - \tau_a^r s_v^q) + \sum_{aqbr} g_{abqr}\left[s_v^r(-\tau_{ab}^{qp} + \tau_{ab}^{pq}) + \tau_a^q s_{bv}^{rp} + \tau_b^q s_{av}^{rp} - \tau_a^q s_{bv}^{pr}\right.\\ &\left.+ \tau_a^p s_{bv}^{qr} - \tau_b^p s_{av}^{qr} + \tau_b^q s_{av}^{pr} + (-\tau_b^p t_a^q - \tau_a^q t_b^p + \tau_b^q t_a^p + \tau_a^p t_b^q)s_v^r\right]\end{aligned} \quad (20)$$

$$\begin{aligned}\langle\overline{\overline{H_N\mathbf{T}^{(1)}}S^{(0)}}\rangle_{va}^{pq} + \langle\overline{\overline{\overline{H_N T^{(0)}}\mathbf{T}^{(1)}}S^{(0)}}\rangle_{va}^{pq} &= \sum_{rs} g_{pqrs}\tau_a^s s_v^r - \sum_{rb}(g_{pbra}\tau_b^q + g_{qbar}\tau_b^p)s_v^r + \sum_{sbr} g_{pbsr}\left[s_v^s(\tau_{ba}^{rq} - \tau_{ab}^{rq}) - s_v^r(\tau_{ab}^{qs}\right.\\ &\left.+ \tau_{ab}^{sp})\right] + \sum_{cbr} g_{cbar}\tau_{cb}^{qp}s_v^r + \sum_{brs} g_{bprs}(s_{va}^{sq}\tau_b^r - s_{va}^{rq}\tau_b^s - s_{bv}^{qs}\tau_a^r - s_{av}^{rs}\tau_b^q - s_{bv}^{pr}\tau_a^s - s_{bv}^{sp}\tau_a^r + s_{sp}^{av}\tau_b^r - s_{rs}^{va}\tau_b^p + s_{bv}^{rp}\tau_a^s\\ &- s_{av}^{rp}\tau_b^s) + \sum_{cbr} g_{cbar}[s_{bv}^{pr}\tau_c^q - s_{cv}^{qp}\tau_b^r + s_{cv}^{rp}\tau_b^q + s_{bv}^{qp}\tau_c^r - s_{bv}^{rp}\tau_c^q + s_{vc}^{rq}\tau_b^p] + \sum_{bcrs} g_{bcrs}\left[s_{cv}^{sp}\tau_{ab}^{qr} + s_{cv}^{rp}\tau_{ab}^{qs} - s_{cv}^{sp}\tau_{ab}^{rq} + s_{cv}^{qp}\tau_{ab}^{rs}\right.\\ &\left.+ s_{av}^{sp}\tau_{bc}^{qr} - s_{cv}^{ps}\tau_{ab}^{qr} + s_{cv}^{rs}\tau_{ab}^{qp} + s_{vc}^{rp}\tau_{ab}^{qs} + s_{vc}^{sp}\tau_{ab}^{rq} - s_{vc}^{rs}\tau_{ab}^{qp} - s_{av}^{sp}\tau_{bc}^{rq} - s_{cv}^{qp}\tau_{ba}^{rs}\right]\end{aligned} \quad (21)$$

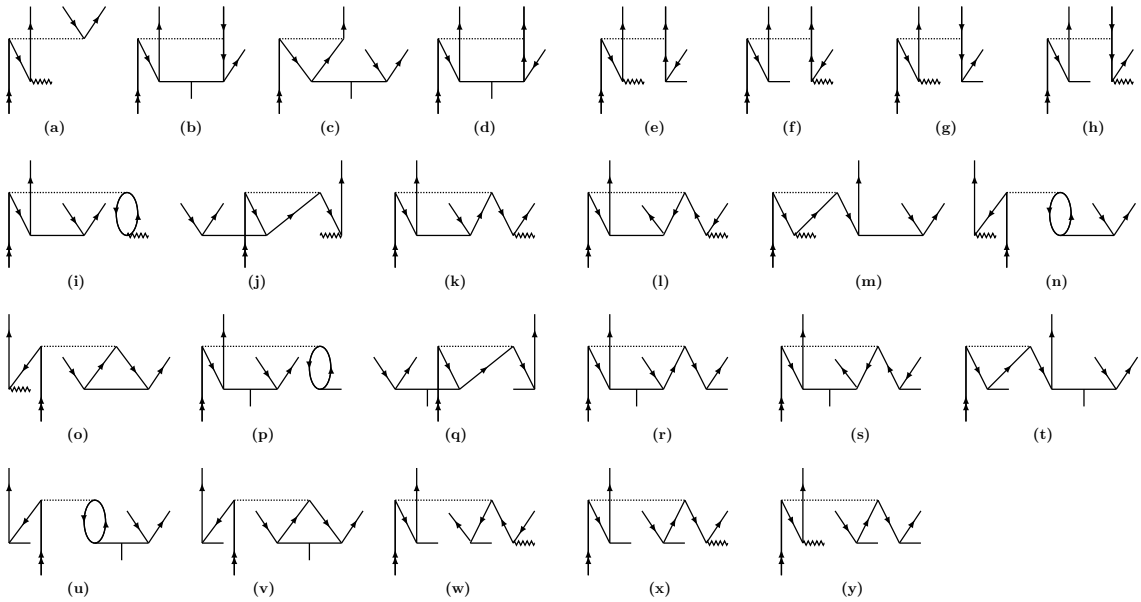

FIG. 5. Double PRCC diagrams contributing to the term $\overline{\bar{H}_N\mathbf{T}}^{(1)}$ of Eq. (11b).

$$\langle\overline{\overline{\overline{H_N T^{(0)}}\mathbf{T}^{(1)}}S^{(0)}}\rangle_{va}^{pq} + \langle\overline{\overline{\overline{H_N T^{(0)}}\mathbf{T}^{(1)}}S^{(0)}}\rangle_{va}^{pq} = \sum_{brs} g_{bprs}\,[(-t_a^r\tau_b^q - t_b^q\tau_a^r)s_v^s - (t_a^s\tau_b^p + t_b^p\tau_a^s)s_v^r] + \sum_{brc} g_{bcar}(t_b^q\tau_c^p + t_c^p\tau_b^q)s_v^r + \sum_{brcs} g_{bcrs}\,[(-t_{ab}^{qr}\tau_c^p + t_{ab}^{qp}\tau_c^r)s_v^s + (-t_{ab}^{qp}\tau_c^s + t_{ab}^{qs}\tau_c^p)s_v^r + (t_{ab}^{rq}\tau_c^p + t_{ac}^{rp}\tau_b^q + t_{bc}^{qp}\tau_a^r)s_v^s + (\tau_{ab}^{qs}t_c^p - \tau_{ab}^{qr}t_c^p + \tau_{ab}^{qp}t_c^r - \tau_{ac}^{qp}t_b^r + \tau_{ac}^{rp}t_b^q + \tau_{bc}^{qp}t_a^r + \tau_{ab}^{rq}t_c^p)s_v^s + [-t_b^r\tau_c^p - t_c^p\tau_b^r + t_b^p\tau_c^r + \tau_b^p t_c^r]s_{va}^{sq} + (-t_b^q\tau_a^r - \tau_b^q t_a^r)s_{cv}^{sp} + (t_c^r\tau_b^q + \tau_c^r t_b^q)s_{av}^{sp} + (t_b^s\tau_a^r + \tau_b^s t_a^r)s_{cv}^{qp} + (t_a^r\tau_b^q + \tau_a^r t_b^q)s_{cv}^{ps} + (t_a^r\tau_c^p + \tau_a^r t_c^p)s_{bv}^{qs} + (t_b^q\tau_c^p + \tau_b^q t_c^p)s_{av}^{rs}] \tag{22}$$

In the case of the PRCC equation for $\mathbf{S}_2^{(1)}$, there are 72 Goldstone diagrams arise from this term. Out of these, 36 diagrams each arise from the first and second terms. These diagrams are shown in the left and right panels, respectively, of the Fig. 7. The algebraic expression of the diagrams in the left panel is given in Eq.(21). Similarly, the algebraic expression of the diagrams in the right panel is given in Eq.(22).

5. $\bar{H}_N\mathbf{S}^{(1)}$

This term contains a perturbed operator, $\mathbf{S}^{(1)}$, which subsumes dominant effects of perturbation for one-valence atomic systems. Expanding $\bar{H}_N$

$$\overline{\bar{H}_N\mathbf{S}}^{(1)} = \overline{H_N\mathbf{S}}^{(1)} + \overline{\overline{H_N T^{(0)}}\mathbf{S}}^{(1)} + \frac{1}{2!}\overline{\overline{\overline{H_N T^{(0)}}T^{(0)}}\mathbf{S}}^{(1)} \tag{23}$$

In the PRCC equation of $\mathbf{S}_1^{(1)}$, both the one- and two-body CC operators from the first and second terms contribute. From the third term, however, only the term $H_N T_1^{(0)} T_1^{(0)} S_1^{(1)}$ contributes. There are 15 diagrams with contribute to the PRCC equation of $\mathbf{S}_1^{(1)}$, and these are shown in the right panel of Fig. 6. The algebraic expression of these diagrams is given in the Eq.(24).

For the PRCC equation of $\mathbf{S}_2^{(1)}$, there are in total 59 diagrams. Out of these 29 diagrams arise from the first two terms. And, these diagrams are shown in the left panel of the Fig. 8. The remaining 30 diagrams arise from the third term, and are shown in the right panel of the Fig. 8. The algebraic expression of diagrams in the left and right panels are given in Eqs. (25) and (26), respectively.

$$\langle\overline{H_N\mathbf{S}}^{(1)}\rangle_v^p + \langle\overline{\overline{H_N T^{(0)}}\mathbf{S}}^{(1)}\rangle_v^p + \langle\overline{\overline{\overline{H_N T^{(0)}}T^{(0)}}\mathbf{S}}^{(1)}\rangle_v^p = \sum_{aqr} g_{apqr}(\xi_{av}^{qr} - \xi_{av}^{rq} + t_a^q\xi_v^r - t_a^r\xi_v^q) + \sum_{aqbr} g_{abqr}[(-t_{ab}^{qp} + t_{ab}^{pq})\xi_v^r + t_a^q\xi_{bv}^{rp} + t_b^q\xi_{av}^{rp} - t_a^q\xi_{bv}^{pr} + t_a^p\xi_{bv}^{qr} - t_b^p\xi_{av}^{qr} + t_b^q\xi_{av}^{pr} + \frac{1}{2!}(-t_a^q t_b^p + t_a^p t_b^q)\xi_v^r + \sum_q g_q^p\xi_v^q \tag{24}$$

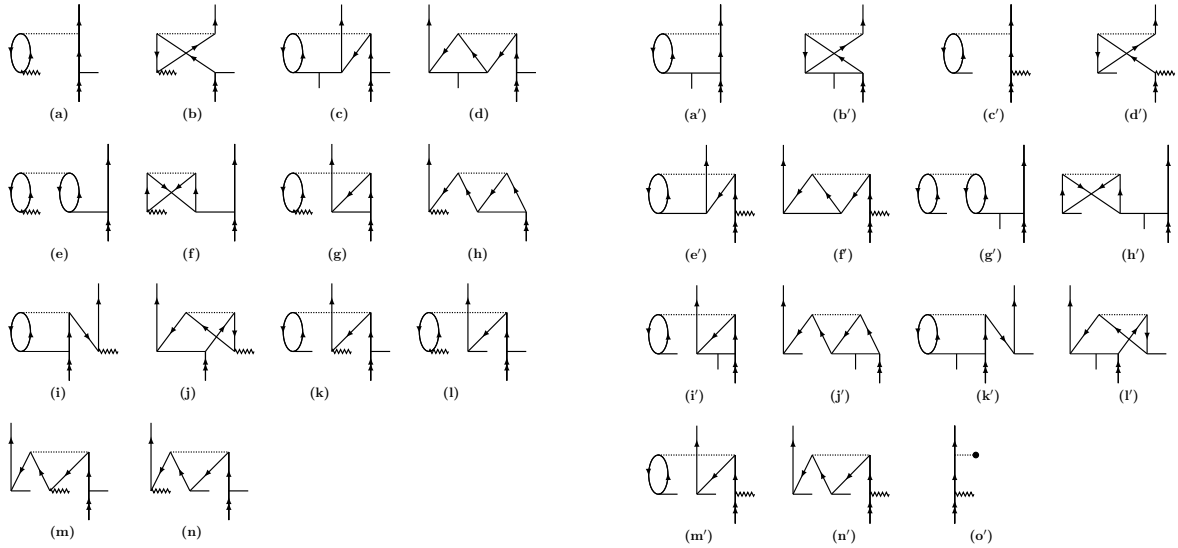

FIG. 6. Single PRCC diagrams contributing to the terms $\overline{\overline{H_N \mathbf{T}^{(1)}} S^{(0)}}$ (panel (a)) and $\overline{H_N \mathbf{S}^{(1)}}$ (panel (b)) of Eq. (11a).

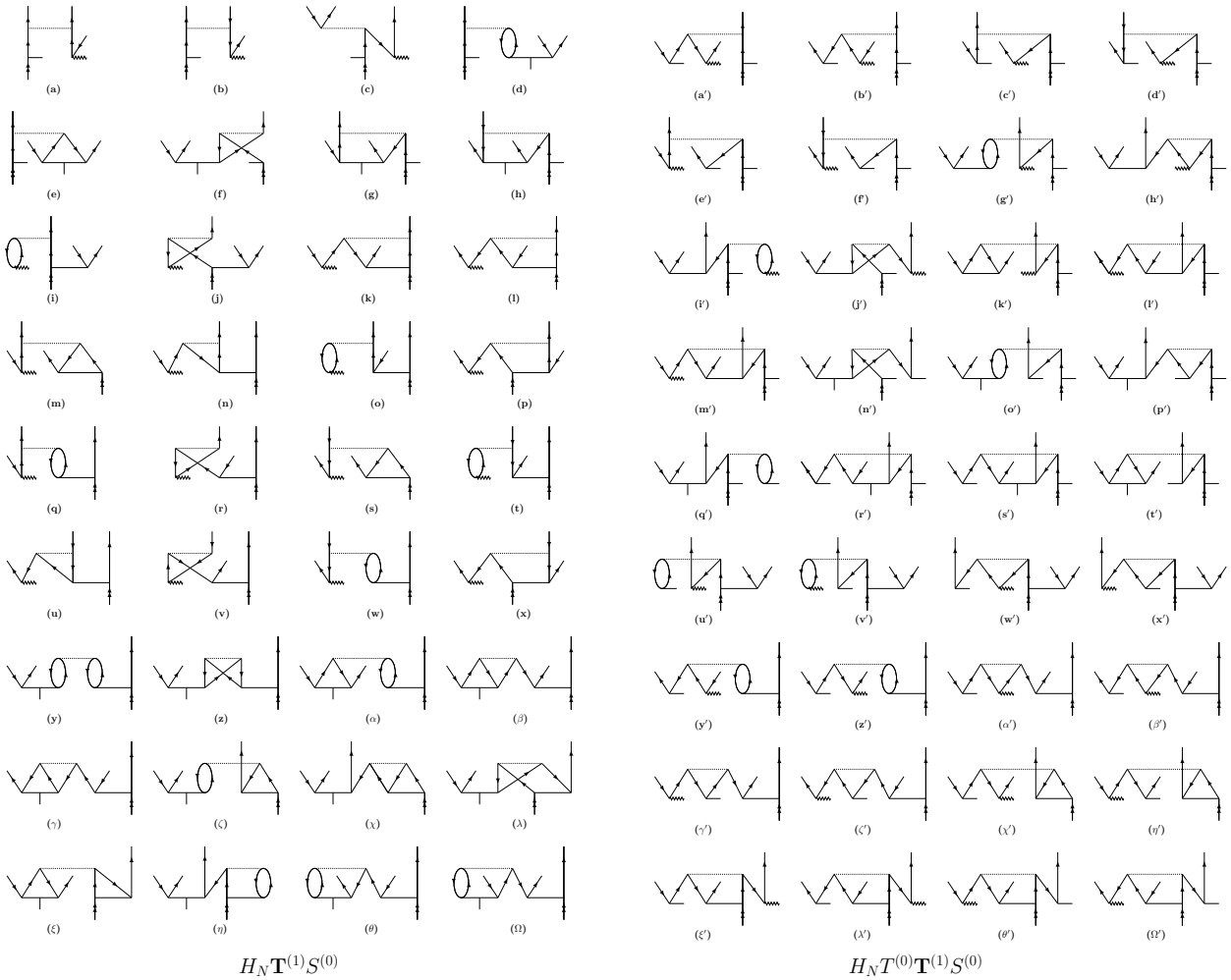

FIG. 7. Double PRCC diagrams contributing to the terms $\overline{\overline{H_N \mathbf{T}^{(1)}} S^{(0)}}$ (left panel) and $\overline{\overline{H_N T^{(0)} \mathbf{T}^{(1)}} S^{(0)}}$ (right panel) of Eq. (11b).

$$\langle \overline{H_N \mathbf{S}^{(1)}} \rangle^{pq}_{va} + \langle \overline{\overline{H_N T^{(0)}} \mathbf{S}^{(1)}} \rangle^{pq}_{va} = \sum_r g_{pqra}\xi^r_v + \sum_{rs} g_{pqrs}\xi^{rs}_{va} - \sum_{rb}(g_{pbra}\xi^{rq}_{vb}$$
$$+ g_{bqar}\xi^{pr}_{vb}) + \sum_{br}\left[-t^p_b g_{qbar} - t^q_b g_{pbra}\right]\xi^r_v + \sum_{rs} g_{pqrs} t^s_a \xi^r_v + \sum_{bsr}\left[g_{bpsr}(t^s_b\xi^{rq}_{va} - t^r_b\xi^{sq}_{va} - t^s_a\xi^{qr}_{bv} - t^q_b\xi^{sr}_{av}) + g_{bqsr}(t^r_a\xi^{sp}_{bv}\right.$$
$$\left. - t^p_b\xi^{sr}_{va} - t^r_a\xi^{ps}_{bv} - t^s_a\xi^{rp}_{bv} + t^s_b\xi^{rp}_{av} - t^r_b\xi^{sp}_{av})\right] + \sum_{rbc} g_{bcra}\left[t^r_c\xi^{qp}_{bv} - t^r_b\xi^{qp}_{cv} + t^q_c\xi^{pr}_{bv} + t^q_b\xi^{rp}_{cv} + t^p_b\xi^{rq}_{vc} - t^q_c\xi^{rp}_{bv} + t^{qp}_{cb}\xi^r_v\right]$$
$$+ g_{pbsr}\left[(t^{rq}_{ba} - t^{rq}_{ab})\xi^s_v - t^{qs}_{ab}\xi^r_v\right] - g_{qbsr}t^{sp}_{ab})\xi^r_v] + \sum_r g_{pr}t^{rq}_{va} \tag{25}$$

$$\langle \overline{\overline{H_N T^{(0)}} T^{(0)} \mathbf{S}^{(1)}} \rangle^{pq}_{va} = \sum_{brcs} g_{bcrs}\left[(t^{qr}_{ab} - t^{rq}_{ab})\xi^{sp}_{cv} + t^{qs}_{ab}\xi^{rp}_{cv} + t^{rs}_{ab}\xi^{qp}_{cv} + t^{qr}_{bc}\xi^{sp}_{av} - t^{qr}_{ab}\xi^{ps}_{cv} + t^{qp}_{ab}(\xi^{rs}_{cv} - \xi^{rs}_{vc})\right.$$
$$\left. + t^{rq}_{ab}\xi^{sp}_{vc} + t^{qs}_{ab}\xi^{rp}_{vc} - t^{rq}_{bc}\xi^{sp}_{av} - t^{rs}_{ba}\xi^{qp}_{cv}\right] + \sum_{rbs}\left[-g_{bprs}t^r_a t^q_b \xi^s_v - g_{bqrs}t^s_a t^p_b \xi^r\right] + \sum_{cbr} g_{cbar}t^q_c t^p_b \xi^r_v + \sum_{brcs} g_{bcrs}[(-t^{qr}_{ab}t^p_c$$
$$+ t^{qp}_{ab}t^r_c)\xi^s_v + (-t^{qp}_{ab}t^s_c + t^{qs}_{ab}t^p_c)\xi^r_v + (t^{rp}_{ac}t^q_b + t^{qp}_{bc}t^r_a + t^{rq}_{ab}t^p_c)\xi^s_v + (t^q_b\xi^{rs}_{av} + t^r_a\xi^{qs}_{bv} - t^r_b\xi^{sq}_{va})t^p_c + t^p_b\xi^{sq}_{va}t^r_c + t^r_a(-t^q_b\xi^{sp}_{cv}$$
$$+ t^s_b\xi^{qp}_{cv}) + t^q_b(t^r_c\xi^{sp}_{av} + t^r_a\xi^{ps}_{cv}). \tag{26}$$

6. *Folded diagrams*

The terms on the right-hand sides of the PRCC Eqs.(11a) and (11b) are referred to as the renormalization terms in the CC equation of the one-valence systems. It is an important term, and its nonzero value distinguishes the PRCC equations of open-shell systems from the closed-shell systems. These contribute through the folded diagrams arising from the contraction of the energy with the CC operators. This contraction is not possible in the case of closed-shell systems as the energy diagrams do not have free lines. Folded diagrams contributing to Eqs. (11a) and (11b) are given in Fig. 9 as diagrams (a) and (b), respectively.

III. POLARIZABILITY FOR ONE-VALENCE USING PRCC

In the PRCC, the electric dipole polarizability α of an atom or ion is defined as the expectation of the dipole operator with respect to the perturbed state $|\tilde{\Psi}_v\rangle$. For the one-valence atomic system

$$\alpha = -\frac{\langle\tilde{\Psi}_v|\mathbf{D}|\tilde{\Psi}_v\rangle}{\langle\Psi_v|\Psi_v\rangle} \tag{27}$$

Using the expression of $|\tilde{\Psi}_v\rangle$ from Eq. (5) and retaining only the terms with first-order in λ, we get

$$\alpha = \frac{1}{\mathcal{N}}\langle\Phi_v|\bar{\mathbf{D}}\left(\mathbf{S}^{(1)} + \mathbf{T}^{(1)} + \mathbf{T}^{(1)}S^{(0)}\right) + \left(\mathbf{S}^{(1)} + \mathbf{T}^{(1)}\right.$$
$$\left. + \mathbf{T}^{(1)}S^{(0)}\right)^\dagger \bar{\mathbf{D}} + S^{(0)\dagger}\bar{\mathbf{D}}\left(\mathbf{S}^{(1)} + \mathbf{T}^{(1)} + \mathbf{T}^{(1)}S^{(0)}\right)$$
$$+ \left(\mathbf{S}^{(1)} + \mathbf{T}^{(1)} + \mathbf{T}^{(1)}S^{(0)}\right)^\dagger \bar{\mathbf{D}}S^{(0)}|\Phi_v\rangle, \tag{28}$$

where

$$\mathcal{N} = \langle\Phi_v|(e^{T^{(0)}}(1 + S^{(0)}))^\dagger(e^{T^{(0)}}(1 + S^{(0)}))|\Phi_v\rangle, \tag{29}$$

is the normalization factor of the eigenstate $|\Psi_v\rangle$ and $\bar{\mathbf{D}}, = e^{T^{(0)\dagger}}\mathbf{D}e^{T^{(0)}}$, is a dressed operator, which is a nonterminating series of the cluster operator $T^{(0)}$. In the present work, however, we consider up to to the second order term $\bar{\mathbf{D}} = \mathbf{D} + \mathbf{D}T^{(0)} + T^{(0)\dagger}\mathbf{D} + T^{(0)\dagger}\mathbf{D}T^{(0)}$. The higher order terms in $T^{(0)}$ have negligible contributions and this has been confirmed through detailed computations [40]. In the CCSD approximation, Eq. (28) can be written as

$$\alpha = \frac{1}{\mathcal{N}}\langle\Phi_v|\left(\mathbf{DS}^{(1)}_1 + \mathbf{DS}^{(1)}_2 + S^{(0)\dagger}_1\mathbf{DS}^{(1)}_1 + S^{(0)\dagger}_1\mathbf{DS}^{(1)}_2 + S^{(0)\dagger}_2\mathbf{DS}^{(1)}_1 + S^{(0)\dagger}_2\mathbf{DS}^{(1)}_2 + S^{(0)\dagger}_1\mathbf{DT}^{(1)}_1 + S^{(0)\dagger}_2\mathbf{DT}^{(1)}_1\right.$$
$$+ S^{(0)\dagger}_2\mathbf{DT}^{(1)}_2 + T^{(0)\dagger}_1\mathbf{DS}^{(1)}_1 + T^{(0)\dagger}_1\mathbf{DS}^{(1)}_2 + T^{(0)\dagger}_2\mathbf{DS}^{(1)}_2 + \mathbf{DT}^{(1)} + T^{(0)\dagger}_1\mathbf{DT}^{(1)}_1 + T^{(0)\dagger}_1\mathbf{DT}^{(1)}_2 + T^{(0)\dagger}_2\mathbf{DT}^{(1)}_1$$
$$\left. + T^{(0)\dagger}_2\mathbf{DT}^{(1)}_2\right) + \text{H.c} + \mathbf{DT}^{(1)}_1 S^{(0)}_1 + \mathbf{DT}^{(0)}_1\mathbf{S}^{(1)}_1|\Phi_v\rangle. \tag{30}$$

Here, the terms $S^{(0)\dagger}_1\mathbf{DT}^{(1)}_2$ + H.c., $T^{(0)\dagger}_2\mathbf{DS}^{(1)}_2$ + H.c. and $\mathbf{DT}^{(1)}_2$ + H.c. are not included as these do not contribute to the α of the one-valence system.

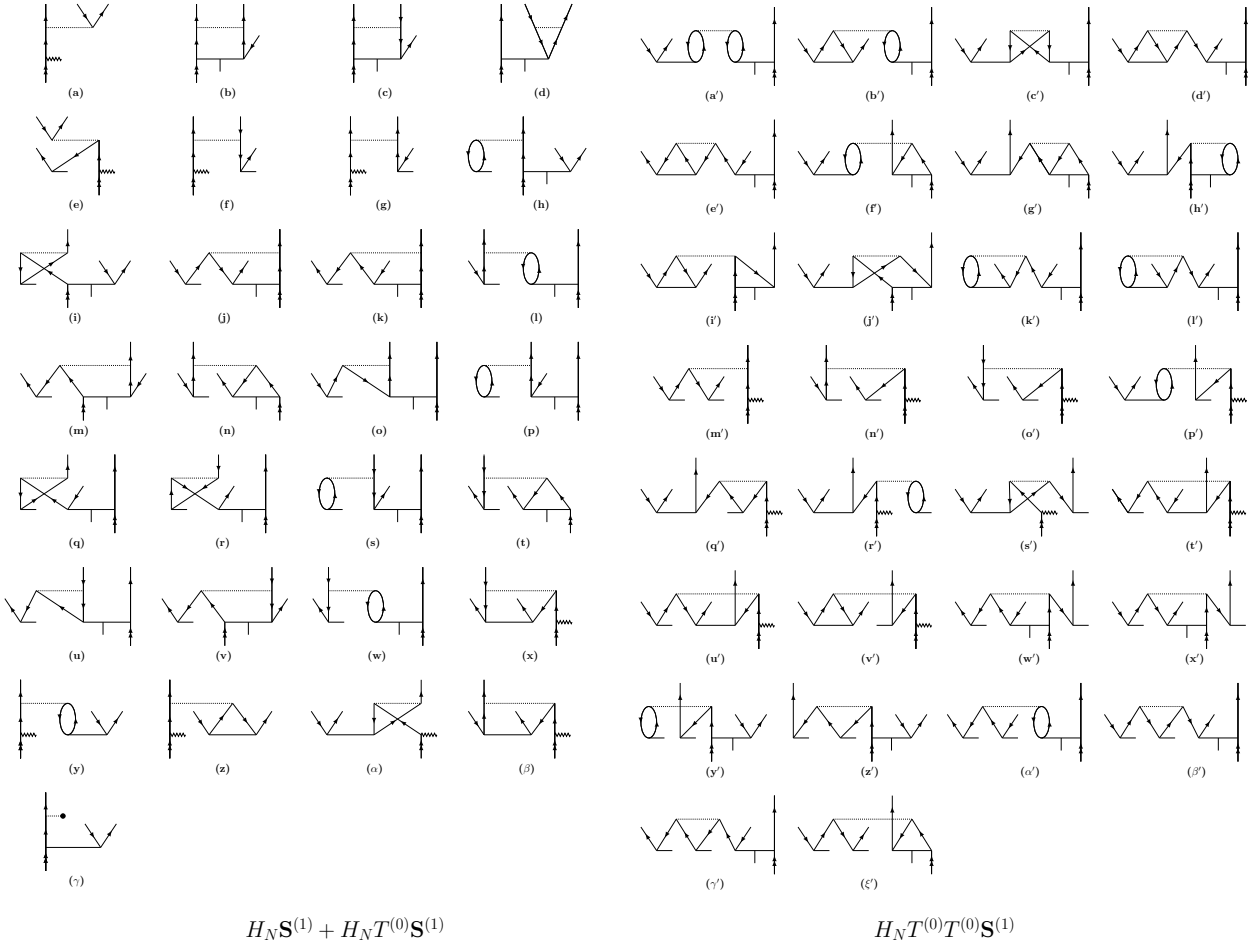

FIG. 8. Double PRCC diagrams contributing to the terms $\overline{H_N\mathbf{S}}^{(1)} + \overline{H_N T^{(0)}\mathbf{S}}^{(1)}$ (left panel) and $\overline{H_N T^{(0)} T^{(0)}\mathbf{S}}^{(1)}$ (right panel) of Eq. (11b).

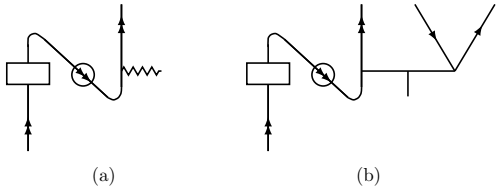

FIG. 9. Folded diagrams contributing to PRCC Eqs. (11a) (diagram (a)) and (11b) (diagram (b)).

A. Diagrams for α

There are 128 Goldstone diagrams which contribute to the Eq. (30). And as example of the diagrams, in Fig. 10, we show one diagram from each of the terms in the Eq. (30). The diagrams from the Hermitian conjugate terms are, however, not shown as these are topologically equivalent. Among all the terms in the Eq. (30), the first four terms, $\mathbf{DS}_1^{(1)}$, $\mathbf{DS}_2^{(1)}$ and their hermitian conjugates, are expected to have the dominant contribution. The reason for this is the large magnitude of the one-valence cluster operators and the strong effect of the perturbation on these operators. More importantly, the terms $\mathbf{DS}_1^{(1)}$+H.c. subsumes the contributions from the Dirac-Fock (DF) and the random-phase-approximation (RPA). The diagrams of the $\mathbf{DS}_1^{(1)}$ and $\mathbf{DS}_2^{(1)}$ are shown in Fig. 10(a) and (b), respectively.

Among the terms with two-orders of CC operators, $S_1^{(0)\dagger}\mathbf{DS}_1^{(1)}$, $S_1^{(0)\dagger}\mathbf{DS}_2^{(1)}$, $S_2^{(0)\dagger}\mathbf{DS}_1^{(1)}$, $S_2^{(0)\dagger}\mathbf{DS}_2^{(1)}$ and their H.c., are expected to give dominant contributions. The example diagrams of these four terms are shown in the Fig. 10(c-f). The next important contributions are expected from the terms with one each of the T and S operators; $S_1^{(0)\dagger}\mathbf{DT}_1^{(1)}$, $S_2^{(0)\dagger}\mathbf{DT}_1^{(1)}$, $S_2^{(0)\dagger}\mathbf{DT}_2^{(1)}$, $T_1^{(0)\dagger}\mathbf{DS}_1^{(1)}$, $T_1^{(0)\dagger}\mathbf{DS}_2^{(1)}$, $T_2^{(0)\dagger}\mathbf{DS}_2^{(1)}$ and their H.c., and $\mathbf{DT}_1^{(1)}S_1^{(0)}$ and $\mathbf{D}T_1^{(0)}\mathbf{S}_1^{(1)}$. The representative diagrams from these terms are shown in Fig.10(g-n). The remaining terms, $\mathbf{DT}_1^{(1)}$, $T_1^{(0)\dagger}\mathbf{DT}_1^{(1)}$, $T_1^{(0)\dagger}\mathbf{DT}_2^{(1)}$, $T_2^{(0)\dagger}\mathbf{DT}_1^{(1)}$, $T_2^{(0)\dagger}\mathbf{DT}_2^{(1)}$ and their H.c., having two-orders of closed-shell operator, are expected to have the lowest contribution to α. This is due to the small magnitudes of these operators for the open-shell systems. Some representative diagrams from these are shown in Fig.10(o-s).

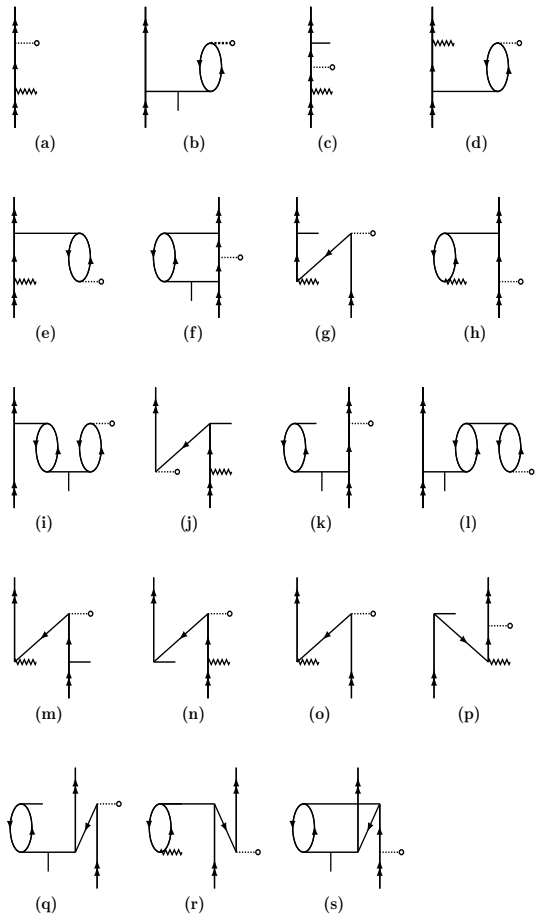

FIG. 10. Some example polarizability diagrams for one-valence atomic system, contributing to Eq. (30)

.

IV. BASIS SET CONVERGENCE

A basis set which provides a good description of the single-electron wave functions and energies is essential to obtain accurate and reliable results using the PRCC theory. In this work, we have used Gaussian-type orbitals (GTOs) [37] as the single-electron basis set. To ensure the accuracy of the basis set, the basis parameters are optimized to match the orbital energies as well as the self-consistent-field energies with the GRASP2K [45] results. We achieved an excellent agreement between the GTO and GRASP2K energies. A detailed analysis and comparison of the energies of the group-13 elements is reported in our recent work [31]. To improve the quality of the basis set further, we incorporate the effects of Breit interaction, vacuum polarization (VP) and the self-energy (SE) corrections in the basis set generation. For the Breit interaction, we employ the expression given in Ref. [46] and incorporate it at the level of orbital basis as well as the PRCC calculations. The effects of the vacuum polarization is considered using the Uehling potential [47], modified to incorporate the finite size effects of nucleus [48]. The self-energy corrections to the orbitals are incorporated through the model Lamb-shift operator introduced by Shabaev *et al.* [49], and were calculated using the code QEDMOD [50].

TABLE I. Convergence trend of α calculated using the Dirac-Coulomb Hamiltonian as function of basis size.

Basis	Orbitals	α	
		$^2P_{1/2}$	$^2P_{3/2}$
	Al		
98	18s, 18p, 9d, 6f, 4g, 3h	−58.852	−64.185
120	20s, 20p, 11d, 8f, 6g, 5h	−59.433	−65.183
142	22s, 22p, 13d, 10f, 8g, 7h	−58.762	−64.461
164	24s, 24p, 15d, 12f, 10g, 9h	−58.347	−63.985
175	25s, 25p, 16d, 13f, 11g, 10h	−58.273	−63.896
181	27s, 27p, 16d, 13f, 11g, 10h	−58.273	−63.896
	In		
110	18s, 18p, 13d, 6f, 5g, 4h	−67.934	−87.128
132	20s, 20p, 15d, 8f, 7g, 6h	−68.339	−87.489
154	22s, 22p, 17d, 10f, 9g, 8h	−67.203	−86.093
176	24s, 24p, 19d, 12f, 11g, 10h	−64.678	−82.842
187	25s, 25p, 20d, 13f, 12g, 11h	−64.024	−82.036
192	26s, 26p, 21d, 13f, 12g, 11h	−64.027	−81.996
197	27s, 27p, 22d, 13f, 12g, 11h	−64.027	−81.996

Owing to the mathematically incomplete nature of the GTO basis [51], it is essential to check the convergence of properties with the basis size. In Table I, we demonstrate the convergence of α for Al and In by listing α for both the fine structure states as a function of the basis size. For these calculations we have used the Dirac-Coulomb (DC) Hamiltonian as using the DCB Hamiltonian is computationally more expensive. As evident from the table, to achieve the convergence of α, we start with a moderate basis size by considering up to the h symmetry. And, then systematically increase the number of orbitals in each symmetry until the change in α is $\leqslant 10^{-3}$ a.u. For example, in the case of Al, the change in α is 2×10^{-8} a.u. when the basis set is augmented from 175 to 181 orbitals. So, we consider the basis set with the 175 orbitals as the optimal set and use it in further calculations to incorporate the effects of the Breit interaction and QED corrections. The same approach is also adopted to achieve the convergence of excitation energies, however, with a key difference. In this case, the basis set includes orbitals from j-symmetry also. The convergence trends of the excitation energies and α are shown in the Fig. 11 (a) and (b), respectively. As discernible from the figure, both the excitation energy and α converge well with the basis size.

V. RESULTS AND DISCUSSION

A. Excitation energies

The excitation energy of a state $|\Psi_w\rangle$ is defined as

$$\Delta E_w = E_w - E_v, \tag{31}$$

where E_v is the energy of the ground state wavefunction, and obtained from the solution of Eq. (2) for $3p_{1/2}$ and $5p_{1/2}$ states for Al and In, respectively. And, E_w is the energy of an

TABLE II. Energy (cm^{-1}) of the ground state and the excitation energies of low-lying atomic states of Al and In.

States	RCC results	NIST[52]
	Al	
$3s^2\ 3p_{1/2}$	48147.69	48275.20
$3s^2\ 3p_{3/2}$	111.93	112.06
$3s^2\ 4s_{1/2}$	25363.81	25347.76
$3s^2\ 4p_{1/2}$	32927.34	32949.81
$3s^2\ 4p_{3/2}$	32938.49	32965.64
	In	
$5s^2\ 5p_{1/2}$	46633.75	46670.20
$5s^2\ 5p_{3/2}$	2411.59	2212.59
$5s^2\ 6s_{1/2}$	24413.48	24372.96
$5s^2\ 6p_{1/2}$	31864.31	31816.96
$5s^2\ 6p_{3/2}$	32179.48	32115.22
$5s^2\ 5d_{3/2}$	32912.20	32892.21
$5s^2\ 5d_{5/2}$	32921.59	32915.54

excited state $|\Psi_w\rangle$. In the RCC, E_w is given by [40]

$$E_w = \langle\Phi_w|\bar{H}^{\rm DCB}(1+S^{(0)})|\Phi_w\rangle, \tag{32}$$

where $|\Phi_w\rangle$ is an excited Dirac-Fock state. In the Table II, we have listed the energy of the ground state and the excitation energies of a few low-lying states of Al and In. For comparison, the experimental values from NIST [52] are also listed in the table. For Al, our theoretical results are in excellent agreement with the experimental data for all states. The maximum relative error is 0.26%, in the case of $3p_{1/2}$ state. For In also we observe the same trend of relative errors except for the state $5p_{3/2}$, where the error is 9%. This could be attributed to the correlation effects from higher energy configurations not included in the present work due to divergence issues.

To discern the electron correction effects as a function of configurations included in the computations, energies are computed with different configuration spaces in steps. For this we start with the ground state configuration in the configuration space and include the higher energy configurations in subsequent steps. For Al, we start with $3s^23p$ and refer to this as CF1. Then, we include two configurations $3s^24s$ and $3s^24p$ in two subsequent calculations (CF2 and CF3), respectively. The inclusion of the configuration $3s^23d$, however, leads to the divergence in the FSRCC computations due to small energy denominator, and hence, we do not compute the excitation energy of $3d$. For In, $5s^25p$ (CF1) is the starting configuration and the excited state configurations $5s^26s$, $5s^26p$ and $5s^25d$ are included in the later computations with configuration spaces identified as CF2, CF3 and CF4, respectively. The trend of contributions from the higher energy configurations to the ground state energies of Al and In is shown in the Fig. 11(c). As we observe from the figure, for both the atoms, the relative error decreases with the inclusion of higher energy configurations. The reason for this is attributed to the better inclusion of the *core-valence* and *valence-valence* correlations with larger configuration space.

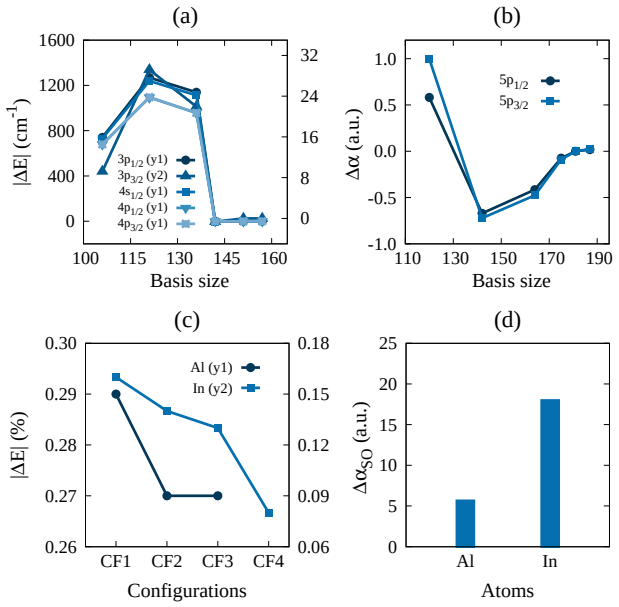

FIG. 11. Convergence of excitation energies (panel (a)) and dipole polarizability (panel (b)) as function of basis size for Al. Percentage change in the ground state energies of Al and In, panel (c). Difference in the α values of spin-orbit splitted states, $^2P_{1/2}$ and $^2P_{3/2}$, of Al and In.

B. Polarizability

We list the value of α for ground state, $^2P_{1/2}$, and SO-coupled excited state, $^2P_{3/2}$, in the Tables III and IV, respectively. For comparison we have also listed the other theoretical and experimental results from previous works. The results listed as PRCC are using the DC Hamiltonian and the converged bases with orbitals $25s25p16d13f11g10h$ and $26s26p21d13f12g11h$ for Al and In, respectively. And, the results listed as PRCC+Breit+QED incorporate the effects of Breit and QED corrections. The values listed as *estimated* refers to the value after incorporating the estimated contributions from the i, j and k-symmetry orbitals. To quantify the effects of electron correlations from the nonlinear terms in the PRCC, the contributions from the DF and LPRCC are provided separately.

From the tables, we observe three important trends in the DF, LPRCC and PRCC α values for Al and In. First, except for the $^2P_{3/2}$ state of In, the LPRCC values are smaller than the DF values. This could be attributed to the contraction of the core with the inclusion of correlation effects within the LPRCC. Second, for both the atoms the PRCC values are larger than the DF. This is due to the contribution of electron correlations from the nonlinear terms. On close examination, we find that the nonlinear terms with one each of the perturbed and unperturbed CC operators, viz, $\overline{H_N\mathbf{T}^{(1)}}S^{(0)}$ and $\overline{H_NT^{(0)}\mathbf{S}^{(1)}}$, contribute the most. And third, the difference between α of the fine-structure states, $\alpha_{\rm FS}$, of In is more than three times larger than Al. This is shown in the Fig. 11(d). The reason for this could be the larger difference in the radial

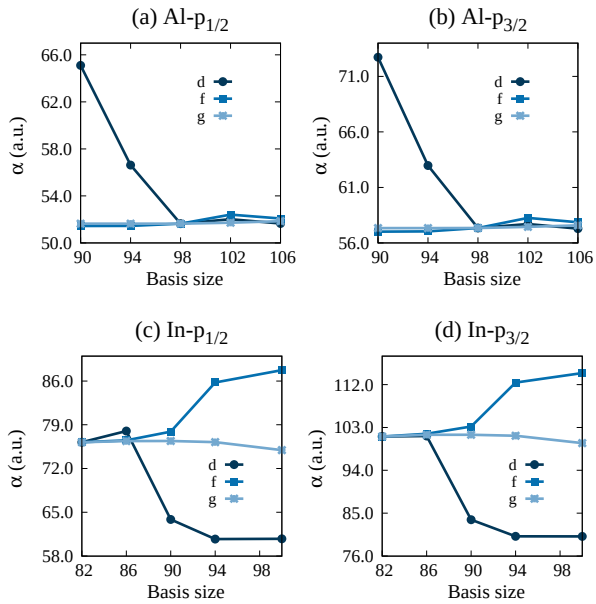

FIG. 12. Trend of contributions to α from virtual orbitals for Al (panels (a) and (b)) and In (panels (c) and (d)) as basis is augmented.

TABLE III. The final value of α (a.u.) for $^2P_{1/2}$ from our calculations compared with the other theory and experimental results.

Our results	Method	Others	Method
		Al	
57.083	DF	55.4 ± 2.2[20]	MRCI
51.537	LPRCC	57.74 [23]	CCSD(T)
58.273	PRCC	57.8 ± 1.0[22]	SI-SOCI
58.690	PRCC+Br.	58.0 ± 0.4[24]	CCSD(T)
58.691	PRCC+Br.+QED	61.0[25]	SCI-DFT
58.697	Est.	46 ± 2[26]	Exp.
58.70(59)	Reco.	55.3 ± 5.5[27]	Exp.
		In	
62.756	DF	61.9 ± 1.2[20]	MRCI
58.544	LPRCC	62.0 ± 1.9[21]	FSCC(T)
64.027	PRCC	61.5 ± 5.6[53]	CCSD(T)
64.246	PRCC+Br.	66.4 ± 5.0[22]	SI-SOCI
64.269	PRCC+Br.+QED	70.3[25]	SCI-DFT
64.228	Est.	68.7 ± 8.1[28]	Exp.
64.23(64)	Reco.	62.1 ± 6.1[29]	Exp.

extents of the $^2P_{1/2}$ and $^2P_{3/2}$ states in In. In the DF computations, $\langle r\rangle_{^2P_{3/2}} - \langle r\rangle_{^2P_{1/2}} = 0.138$ a.u. for In, however, it is only 0.007 a.u. for Al.

1. $^2P_{1/2}$

For $^2P_{1/2}$ of Al, there are two experimental results of α. However, there is a large difference between the reported values. The latest experimental result of α given in the Ref. [27] is $\approx 20\%$ larger than the previous result reported in the Ref. [26]. In addition, there is significant difference in the experimental errors. The measurement in Ref. [27] has an experimental error of $\approx 10\%$, whereas in the Ref. [26] it is $\approx 4\%$. Our recommended value, 58.70, is $\approx 6\%$ larger than the Ref. [27]. From the previous theoretical studies, there are five results for comparison. These include two coupled-cluster results, similar to method we have employed in the present work. However, with a key difference in the calculation of α: the two previous works used finite-field method. Like in the experimental results, here as well, there is a variation in the reported values. There is a difference of about 10% between the lowest [20] and the highest [25] reported values. Although Refs. [20] and [22] adopt the same quantum many-body method, the value in Ref. [22] is larger than Ref. [20]. Our PRCC value, 58.27, is in good agreement with the CCSD(T) calculations, Refs. [23] and [24], and SI-SOCI result [22]. Our recommended value, 58.70, is on the higher side of these results. The reason for this is attributed to the inclusion of the contributions from the Breit and QED corrections and the large basis sets in our calculations. The DF value

For In also there are two experimental results for ground state and, like Al, they differ by large amount – the recent measurement by molecular-beam electric deflection technique [29] is about 10.6% larger value than the Ref. [28]. Our recommended value, 64.23, lies between the two results. Among the previous calculations, in terms of methods adopted, the calculations by Borschevsky *et al.* [21] and Safronova *et al.* [53] are closed to ours. Considering the error bars, our recommended value, 64.23, is in good agreement with these calculations. The reason for a small difference could be attributed to the basis set difference and the contributions from the Breit and QED corrections. The other two results are using the CI based calculations. The result, 66.4, from Ref. [22] is the largest among all the results and differ by about 8% from the smallest value 61.5, Ref. [20].

2. $^2P_{3/2}$

Unlike the $^2P_{1/2}$ state, the static dipole polarizability for $^2P_{3/2}$ state will also have the contributions from the anisotropy components associated with magnetic quantum numbers $M_J = \pm 3/2$ and $\pm 1/2$. In Table IV, we have tabulated the average value, $\bar{\alpha}$, of the polarizability. On close examination of the results, we observe three important differences in the trend of electron correlations in comparison to $^2P_{1/2}$ state. First, for both the atoms, the DF and LPRCC values are very close to each other. This indicates the less contraction of the core orbitals with the inclusion of the electron correlations. Second, the percentage contribution from the nonlinear terms in PRCC is less than $^2P_{1/2}$. And third, the overall Breit+QED correction has increased two-fold.

To the best of our knowledge, for both the atoms, there is no data on α from the experiments for $^2P_{3/2}$. And, from the previous calculations, there are few data from relativistic calculations which are listed in the table. In Refs. [20] and [21], a coupled-cluster method is employed to obtain the energy of Al and In, respectively, and then α is calculated using the

TABLE IV. The value of $\bar{\alpha}(p_{3/2})$ (a.u.) from our calculations compared with the other theory and experimental results.

Our results	Method	Others	Method
	Al		
57.655	DF	55.9 ± 2.2[20]	MRCI
57.421	LPRCC	58.0 ± 1.0[22]	SI-SOCI
63.896	PRCC		
64.703	PRCC+Br.		
64.704	PRCC+Br.+QED		
64.693	Est.		
64.69(65)	Reco.		
	In		
76.157	DF	69.7 ± 1.4[20]	MRCI
76.586	LPRCC	74.4 ± 8.0[22]	SI-SOCI
81.996	PRCC	69.6 ± 3.5[21]	FSCC(T)
82.545	PRCC+Br.		
82.493	PRCC+Br.+QED		
82.500	Est.		
82.50(83)	Reco.		

finite-field approach. In Ref. [22], however, a configuration interaction method is combined with finite-filed approach to calculate the α for In. For Al, our LPRCC result is within the error bars of the Refs. [20, 21]. Our recommended value, 64.69, is however larger than both the references. The reason for this is attributed to the large correlation effects from nonlinear terms in the PRCC theory. A sizable combined contribution from Breit+QED is also observed. The same trend of comparison with previous results is also observed for In. Here, however, there is a variation in the previous results and associated theoretical uncertainties. Our recommend value, 82.50, is within the error bar of the Ref. [22].

C. Electron correlations

Next, we analyze and present the different electron correlations effects incorporated in the calculations of α. For this, we separate the expression in Eq. (30) into six different terms and give their contributions in the Table V. As evident from the table, for both the atoms, the leading order (LO) term is $\mathbf{S}^{(1)\dagger}\mathbf{D}$ + H.c. The contribution from the LO term is $\approx$ 146%(138%) and $\approx$ 141%(131%) of the PRCC value for the $^2P_{1/2}(^2P_{3/2})$ state of Al and In, respectively. That is, the contribution from the LO term exceeds the total value. This is expected as it incorporates the results from the DF term and core-polarization (CP) effects. Except for the $^2P_{3/2}$ of Al, the next leading order (NLO) term is $\mathbf{S}^{(1)\dagger}\mathbf{D}S^{(0)}$ + H.c. It contributes $\approx$ $-10.6\%(-6.5\%)$ and $-13.6\%(-10.8\%)$ for the $^2P_{1/2}(^2P_{3/2})$ state of Al and In, respectively. For the next to NLO contribution, the terms $\mathbf{S}^{(1)\dagger}\mathbf{D}S^{(0)}$ + H.c. and $\mathbf{T}^{(1)\dagger}\mathbf{D}$ + H.c. give nearly equal contributions. Like the NLO term, the contributions from these terms are opposite in phase to the LO contribution, and hence, reduces the total value of α. It is to be mentioned here that the contributions from the core-electrons to α are important. This is unlike the properties of one-valence systems without an external perturbation like the electromagnetic transitions. This is reflected in the contribution from the term $\mathbf{T}^{(1)\dagger}\mathbf{D}$ + H.c. for both the atoms.

TABLE V. Contributions to α (a.u.) from different terms in PRCC theory for Al and In.

Terms + h. c.	Al		In	
	$^2P_{1/2}$	$^2P_{3/2}$	$^2P_{1/2}$	$^2P_{3/2}$
$\mathbf{S}^{(1)\dagger}\mathbf{D}$	85.3337	88.4131	90.0421	107.8206
$\mathbf{S}^{(1)\dagger}\mathbf{D}S^{(0)}$	-9.1048	-5.7448	-12.2584	-11.7265
$T^{(0)\dagger}\mathbf{D}\mathbf{S}^{(1)}$	-1.8365	-2.2499	-0.7316	-0.9715
$S^{(0)\dagger}\mathbf{D}\mathbf{T}^{(1)}$	-7.2333	-7.2820	-5.5342	-5.5331
$\mathbf{T}^{(1)\dagger}\mathbf{D}$	-7.6424	-7.9950	-7.4631	-7.1608
$T^{(0)\dagger}\mathbf{D}\mathbf{T}^{(1)}$	0.9567	1.1739	1.5013	1.5164
Normalization	-0.9636	-0.9744	-0.9767	-0.9768
Total	58.2732	63.8955	64.0271	81.9959

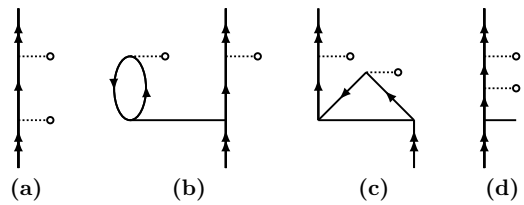

FIG. 13. The DF (diagram (a)), CP (diagrams (b) and (c)) and VC (diagram (d)) terms subsumed in $D\mathbf{S}_1^{(1)}$.

1. Dominant contributions

To gain insights on the dominant contributions from the virtual orbitals, we compute α using basis sets with selective addition of orbitals in d, f and g-symmetries. And, the results are plotted in the Fig. 12. For Al the dominant contribution, as discernible from the figure, is from the d-virtual orbitals. A similar trend in Al^+ was reported in our previous work [31]. The same trend is also observed for In, however, with a key difference. In this case the f-orbitals also contribute. And, this is consistent with the trend reported in our previous work [31] where the f-virtual electrons were found to have dominant contribution due to strong dipolar mixing with the core-electrons in the $4d$ orbital.

To quantify the orbital wise contributions, we identify the dominant cluster amplitudes which contribute to the LO term $\mathbf{D}\mathbf{S}_1^{(1)}$ + H.c. As discernible from the Fig. 14, for Al, at 40.9%(36.6%) the cluster operators with the virtual orbital $3d_{3/2}(3d_{5/2})$ has the largest contribution to the $^2P_{1/2}(^2P_{3/2})$ polarizability. This is due to the strong dipolar mixing between the $3p$ and $3d$ orbitals. The second largest contribution is observed from the cluster amplitudes with the $4s_{1/2}$ virtual orbital, the contribution is $\approx$ 25.3%(24.6%) for the $^2P_{1/2}(^2P_{3/2})$ state. The next three dominant contributions

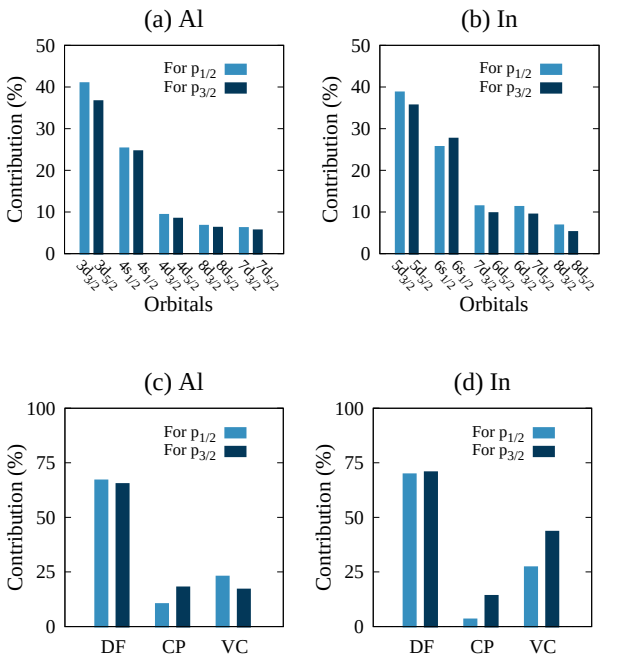

FIG. 14. Five largest percentage contributions to $D\mathbf{S}_1^{(1)}$ + H.c. for $^2P_{1/2}$ and $^2P_{3/2}$ states of Al (panel (a)) and In (panel (b)). The percentage contributions from DF, CP and VC for Al (panel (c)) and In (panel (d)).

are from the $4d$, $8d$ and $7d$ virtual orbitals, and together they contribute $\approx 22.15\%$ (20.18%) for the $^2P_{1/2}(^2P_{3/2})$ state. A similar trend is also observed in the case of In, where the first two dominant contributions are from the $5d$ and $6s$-orbitals. They contribute $\approx 38.7\%$(35.6%) and 25.6%(27.6%), respectively, for the $^2P_{1/2}(^2P_{3/2})$ state. In contrast to Al, the third and fourth dominant contributions are of the same order and different d-electrons contribute to $^2P_{1/2}$ and $^2P_{3/2}$ states.

2. *Core polarization, valence-virtual correlation and QED effects*

Next we assess the contributions from core polarization and pair correlation effects to α of Al and In. The term $\mathbf{DS}_1^{(1)}$ subsumes the contributions from DF, core-polarization (CP) and valence-virtual correlation (VC) effects. The diagrams contributing to these are shown in Fig. 13. The other dominant contribution to the core-polarization is from the term $\mathbf{DS}_2^{(1)}$, and the corresponding diagram are shown in Fig. 10(b) and its exchange. The contribution from the valence-virtual correlation is estimated by subtracting the contributions of diagrams (a), (b) and (c) in Fig. 13 from $\mathbf{DS}^{(1)}$. The percentage contributions of DF, CP and VC are shown in Fig. 14.

For both the atoms, as to be expected, the DF has the largest contribution. In terms of percentage, it constitutes $\approx$ 66.9%(65.2%) and 69.7%(70.6%) of the $\mathbf{DS}^{(1)}$ contribution for the $^2P_{1/2}(^2P_{3/2})$ state of Al and In, respectively. Between CP and VC, except for $^2P_{3/2}$ state of Al, contribution from VC effect is larger than CP and it is more significant in the case of In. In quantitative terms, it constitutes $\approx$ 22.8%(16.9%) and 27.1%(43.4%) of the $\mathbf{DS}^{(1)}$ for the $^2P_{1/2}(^2P_{3/2})$ state of Al and In, respectively. The CP contributions are $\approx$ 10.3%(17.9%) and 3.2%(13.9%) of the $\mathbf{DS}^{(1)}$ for $^2P_{1/2}(^2P_{3/2})$ state of Al and In. It is, however, to be emphasized that the CP contribution in In is smaller than Al. This indicates a better screening of nuclear potential in In. The VC contribution, on the contrary, is larger than Al.

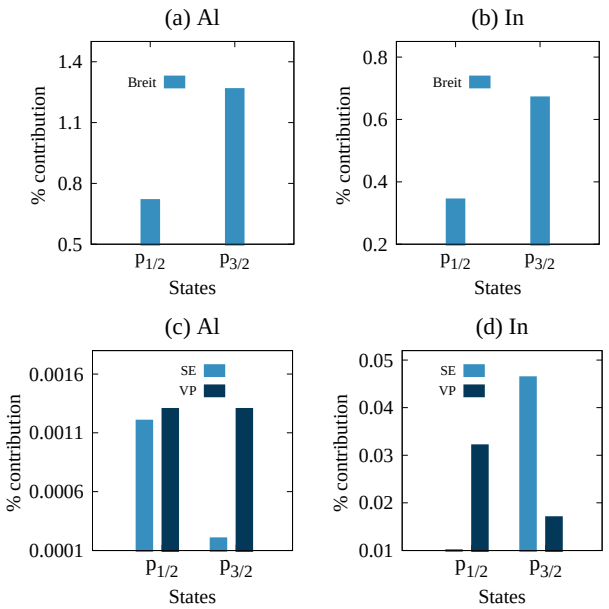

FIG. 15. Contributions from the Breit interaction, vacuum polarization and the self-energy corrections for $^2P_{1/2}$ and $^2P_{3/2}$ states of Al and In.

The contributions from the Breit interaction, vacuum polarization and the self-energy corrections are listed in the Table VI. And, for easy comparison, the contributions in percentage are plotted in the Fig.15. As discernible from the figure, for the both states, the Breit contribution in Al is larger than In. This is consistent with the trend reported in our previous work [31] where we found that, among all the group-13 ions, Al^+ has the highest contribution. The largest contribution is $\approx 1.3\%$ for the $^2P_{3/2}$ state. For the VP and SE contributions, in contrast to the trend of Breit contribution, these are larger in In than Al. The largest contribution from VP is $\approx 0.3\%$ for the $^2P_{1/2}$ state, whereas, SE has the largest contribution of $\approx 0.5\%$, for the case of $^2P_{3/2}$ state of In. The largest combined contribution from Breit interaction and QED corrections is $\approx 1.3\%$, in the case of $^2P_{3/2}$ state of Al. Considering the need of accurate α from theory calculations, this is a significant contribution and can not be ignored.

D. Theoretical uncertainty

Based on the various approximations used in the computations of α, we have identified four sources of uncertainties. The first source of uncertainty is associated with the basis set truncation. From the convergence of α we observe that the

TABLE VI. Contributions to α (a.u.) from Breit interaction, vacuum polarization and the self-energy corrections.

	Al		In	
	$^2P_{1/2}$	$^2P_{3/2}$	$^2P_{1/2}$	$^2P_{3/2}$
DC	58.2732	63.8955	64.0272	81.9959
Breit	0.4172	0.8072	0.2192	0.5490
Self energy	−0.0012	−0.0002	0.0025	−0.0380
Vacuum pol.	0.0013	0.0013	0.0205	−0.0139

change in α, with orbitals up to h-symmetry, is $\leq 10^{-3}$ (a.u.) when the optimal basis set is augmented. And, as listed in the Table IV, the largest overall contribution from the i, j and k symmetry orbitals is in the case of $^2P_{3/2}$ of In and amounts to $\approx 0.06\%$. Although the combined contribution from the orbitals with higher symmetries, beyond the k-symmetry, is expected to be smaller we take 0.1% as an upper bound from this source. The second source of uncertainty is the truncation of the dressed operator $\bar{\mathbf{D}}$ to $\mathbf{D}+\mathbf{D}T^{(0)}+T^{(0)\dagger}\mathbf{D}+T^{(0)\dagger}\mathbf{D}T^{(0)}$. To estimate the uncertainty from this source, we use the findings from our previous work [40] where we showed that the terms with third-order in $T^{(0)}$ and higher together contribute less than 0.1%. We take this as the upper bound from this source. The third source of uncertainty is the truncation of CC operators to singles and doubles. Among the higher excitations, triple excitations contribute the most, and the dominant contribution is subsumed in the perturbative triples. In our previous work [31] on the dipole polarizability of group-13 ions, we had calculated the contributions from perturbative triples to be $\approx 0.06\%$ and 0.28% for Al and In, respectively. Though the cumulative contribution from the missing correlation effects in perturbative triples and higher excitations is expected to be smaller, we take 0.56% as the upper bound from this source of uncertainty. The last source of theoretical uncertainty is associated with the frequency-dependent Breit interaction which is not included in our calculations. To estimate an upper bound of this source we use the results in our previous work [54], where using GRASP2K we estimated an upper bound of 0.13% for Ra. As Al and In are lighter than Ra, the contribution is expected to be smaller, we take 0.13% as the uncertainty from this source. There could be other sources of theoretical uncertainties, such as the higher order coupled perturbation of vacuum polarization and self-energy terms, etc. These, however, have much smaller contributions and their combined uncertainty could be below 0.1%. On combining the upper bounds of all four sources of uncertainties, we estimate a theoretical uncertainty of 1% in the recommended values of α.

VI. CONCLUSION

We have developed a relativistic coupled-cluster theory based method to compute the properties of one-valence atoms and ions with an external perturbation. We employ this method to calculate the electric dipole polarizability of ground state and SO-splitted excited state of Al and In. In addition, to test the quality of the wavefunctions, we also calculated the excitation energy of few low lying states. To improve the accuracy of α further, contributions from the Breit interaction and QED corrections are included. And, to ensure the convergence of α with basis size, large bases up to k-symmetry are used.

For the $^2P_{1/2}$ state, our recommended value lies within the range of the previous theoretical results for both the atoms. In particular, our results are closer to those reported in Refs. [22] and [21] for Al and In, respectively. For the $^2P_{3/2}$ state, however, our recommended value is lager than the previous values. It is to be mentioned that our LPRCC values are closer to the previous results. The reason for the larger PRCC values could be attributed to better inclusion of correlation effects through the inclusion of nonlinear terms.

From the analysis of the electron correlations, we find that for both the atoms, VC contribution is larger than CP. Between Al and In, the contribution from CP decreases, however, VC effects are found to increase. In terms of orbital contributions, for Al, the first two dominant contributions to α come from the $3p-3d$ and $3p-4s$ dipolar mixings. For In, however, they are from the $5p-5d$ and $5p-6s$ mixings. For the contribution from the Breit interaction, the largest contribution is $\approx 1.3\%$ of the DC value, observed in the case of $^2P_{3/2}$ state of Al. And, the largest contributions from the Uehling potential and the self-energy corrections are, $\approx 0.3\%$ and 0.5%, respectively, in the case of $^2P_{1/2}$ and $^2P_{3/2}$ states of In.

ACKNOWLEDGMENTS

We thank Siddhartha Chattopadhyay for useful suggestion on the manuscript. We would also like to thank Chandan, Suraj and Palki for useful discussions. One of the authors, BKM, acknowledges the funding support from the SERB (ECR/2016/001454). The results presented in the paper are based on the computations using the High Performance Computing cluster, Padum, at the Indian Institute of Technology Delhi, New Delhi.

[1] H. G. Dehmelt, "Mono-ion oscillator as potential ultimate laser frequency standard," IEEE Trans. Instrum. Meas. **IM-31**, 83 (1982).

[2] C. W. Chou, D. B. Hume, J. C. J. Koelemeij, D. J. Wineland, and T. Rosenband, "Frequency comparison of two high-accuracy Al^+ optical clocks," Phys. Rev. Lett. **104**, 070802 (2010).

[3] M. S. Safronova, M. G. Kozlov, and Charles W. Clark, "Pre-

cision calculation of blackbody radiation shifts for optical frequency metrology," Phys. Rev. Lett. **107**, 143006 (2011).

[4] Z. Zuhrianda, M. S. Safronova, and M. G. Kozlov, "Anomalously small blackbody radiation shift in the Tl^+ frequency standard," Phys. Rev. A **85**, 022513 (2012).

[5] J.-S. Chen, S. M. Brewer, C. W. Chou, D. J. Wineland, D. R. Leibrandt, and D. B. Hume, "Sympathetic ground state cooling and time-dilation shifts in an $^{27}Al^+$ optical clock," Phys. Rev. Lett. **118**, 053002 (2017).

[6] S. M. Brewer, J.-S. Chen, A. M. Hankin, E. R. Clements, C. W. Chou, D. J. Wineland, D. B. Hume, and D. R. Leibrandt, "$^{27}Al^+$ quantum-logic clock with a systematic uncertainty below 10^{-18}," Phys. Rev. Lett. **123**, 033201 (2019).

[7] S. M. Brewer, J.-S. Chen, K. Beloy, A. M. Hankin, E. R. Clements, C. W. Chou, W. F. McGrew, X. Zhang, R. J. Fasano, D. Nicolodi, H. Leopardi, T. M. Fortier, S. A. Diddams, A. D. Ludlow, D. J. Wineland, D. R. Leibrandt, and D. B. Hume, "Measurements of $^{27}Al^+$ and $^{25}Mg^+$ magnetic constants for improved ion-clock accuracy," Phys. Rev. A **100**, 013409 (2019).

[8] William Arie van Wijngaarden, "Precision measurements of atomic polarizabilities," AIP Conference Proceedings **477**, 305–321 (1999), https://aip.scitation.org/doi/pdf/10.1063/1.59362.

[9] I.B. Khriplovich, *Parity Nonconservation in Atomic Phenomena* (Gordon and Breach Science Publishers, Philadelphia, 1991).

[10] W. C. Griffith, M. D. Swallows, T. H. Loftus, M. V. Romalis, B. R. Heckel, and E. N. Fortson, "Improved limit on the permanent electric dipole moment of Hg^{199}," Phys. Rev. Lett. **102**, 101601 (2009).

[11] M. H. Anderson, J. R. Ensher, M. R. Matthews, C. E. Wieman, and E. A. Cornell, "Observation of Bose-Einstein condensation in a dilute atomic vapor," Science **269**, 198–201 (1995).

[12] C. C. Bradley, C. A. Sackett, J. J. Tollett, and R. G. Hulet, "Evidence of Bose-Einstein condensation in an atomic gas with attractive interactions," Phys. Rev. Lett. **75**, 1687–1690 (1995).

[13] K. B. Davis, M. O. Mewes, M. R. Andrews, N. J. van Druten, D. S. Durfee, D. M. Kurn, and W. Ketterle, "Bose-Einstein condensation in a gas of sodium atoms," Phys. Rev. Lett. **75**, 3969–3973 (1995).

[14] M. Lewenstein, Ph. Balcou, M. Yu. Ivanov, Anne L'Huillier, and P. B. Corkum, "Theory of high-harmonic generation by low-frequency laser fields," Phys. Rev. A **49**, 2117–2132 (1994).

[15] Maciej Lewenstein, Pascal Salières, and Anne L'Huillier, "Phase of the atomic polarization in high-order harmonic generation," Phys. Rev. A **52**, 4747–4754 (1995).

[16] C. I. Blaga, F. Catoire, P. Colosimo, G. G. Paulus, H. G. Muller, P. Agostini, and L. F. DiMauro, "Strong-field photoionization revisited," Nature Phys. **5**, 335 (2009).

[17] Yu Hang Lai, Cosmin I. Blaga, Junliang Xu, Harald Fuest, Philipp Rupp, Matthias F. Kling, Pierre Agostini, and Louis F. DiMauro, "Polarizability effect in strong-field ionization: Quenching of the low-energy structure in C_{60}," Phys. Rev. A **98**, 063427 (2018).

[18] S. G. Karshenboim and E Peik, *Astrophysics, Clocks and Fundamental Constants, Lecture Notes in Physics* (Springer, New York, 2010).

[19] M. T. Murphy, J. K. Webb, and V. V. Flambaum, "Comment on "limits on the time variation of the electromagnetic fine-structure constant in the low energy limit from absorption lines in the spectra of distant quasars"," Phys. Rev. Lett. **99**, 239001 (2007).

[20] Timo Fleig, "Spin-orbit-resolved static polarizabilities of group-13 atoms: Four- component relativistic configuration interaction and coupled cluster calculations," Phys. Rev. A **72**, 052506 (2005).

[21] Anastasia Borschevsky, Tamar Zelovich, Ephraim Eliav, and Uzi Kaldor, "Precision of calculated static polarizabilities: Ga, In and Tl atoms," Chemical Physics **395**, 104 – 107 (2012), recent Advances and Applications of Relativistic Quantum Chemistry.

[22] A. A. Buchachenko, "State-interacting spin-orbit configuration interaction method for J- resolved anisotropic static dipole polarizabilities: Application to Al, Ga, In, and Tl atoms," Russian Journal of Physical Chemistry A **84**, 2325–2333 (2010).

[23] Concetta Lupinetti and Ajit J. Thakkar, "Polarizabilities and hyperpolarizabilities for the atoms Al, Si, P, S, Cl, and Ar: Coupled cluster calculations," The Journal of Chemical Physics **122**, 044301 (2005), https://doi.org/10.1063/1.1834512.

[24] P. Fuentealba, "The static dipole polarizability of aluminium atom: discrepancy between theory and experiment," Chemical Physics Letters **397**, 459 – 461 (2004).

[25] X. Chu and A. Dalgarno, "Linear response time-dependent density functional theory for van der waals coefficients," The Journal of Chemical Physics **121**, 4083–4088 (2004), https://doi.org/10.1063/1.1779576.

[26] Paolo Milani, I. Moullet, and Walt A. de Heer, "Experimental and theoretical electric dipole polarizabilities of Al and Al_2," Phys. Rev. A **42**, 5150–5154 (1990).

[27] G. S. Sarkisov, I. L. Beigman, V. P. Shevelko, and K. W. Struve, "Interferometric measurements of dynamic polarizabilities for metal atoms using electrically exploding wires in vacuum," Phys. Rev. A **73**, 042501 (2006).

[28] T. P. Guella, Thomas M. Miller, B. Bederson, J. A. D. Stockdale, and B. Jaduszliwer, "Polarizability of $5s^2 5p(^2p_{\frac{1}{2}})$ atomic indium," Phys. Rev. A **29**, 2977–2980 (1984).

[29] Lei Ma, John Indergaard, Baiqian Zhang, Ilia Larkin, Ramiro Moro, and Walt A. de Heer, "Measured atomic ground-state polarizabilities of 35 metallic elements," Phys. Rev. A **91**, 010501 (2015).

[30] B.K. Mani, S. Chattopadhyay, and D. Angom, "Rccpac: A parallel relativistic coupled-cluster program for closed-shell and one-valence atoms and ions in fortran," Computer Physics Communications **213**, 136 – 154 (2017).

[31] Ravi Kumar, S. Chattopadhyay, B. K. Mani, and D. Angom, "Electric dipole polarizability of group-13 ions using perturbed relativistic coupled-cluster theory: Importance of nonlinear terms," Phys. Rev. A **101**, 012503 (2020).

[32] Ravi Kumar, S. Chattopadhyay, D. Angom, and B. K. Mani, "Fock-space relativistic coupled-cluster calculation of a hyperfine-induced $^1S_0 \rightarrow {}^3P_0^o$ clock transition in al^+," Phys. Rev. A **103**, 022801 (2021).

[33] M. S. Safronova, W. R. Johnson, and A. Derevianko, "Relativistic many-body calculations of energy levels, hyperfine constants, electric-dipole matrix elements, and static polarizabilities for alkali-metal atoms," Phys. Rev. A **60**, 4476–4487 (1999).

[34] A. Derevianko, W. R. Johnson, M. S. Safronova, and J. F. Babb, "High-precision calculations of dispersion coefficients, static dipole polarizabilities, and atom-wall interaction constants for alkali-metal atoms," Phys. Rev. Lett. **82**, 3589–3592 (1999).

[35] J Mitroy, M S Safronova, and Charles W Clark, "Theory and applications of atomic and ionic polarizabilities,"

Journal of Physics B: Atomic, Molecular and Optical Physics **43**, 202001 (2010).

[36] Peter Schwerdtfeger and Jeffrey K. Nagle, "2018 table of static dipole polarizabilities of the neutral elements in the periodic table," Molecular Physics **117**, 1200–1225 (2019), https://doi.org/10.1080/00268976.2018.1535143.

[37] A. K. Mohanty, F. A. Parpia, and E. Clementi, "Kinetically balanced geometric gaussian basis set calculations for relativistic many-electron atoms," in *Modern Techniques in Computational Chemistry: MOTECC-91*, edited by E. Clementi (ESCOM, 1991).

[38] Richard E. Stanton and Stephen Havriliak, "Kinetic balance: A partial solution to the problem of variational safety in dirac calculations," J. Chem. Phys. **81**, 1910–1918 (1984).

[39] B. K. Mani, K. V. P. Latha, and D. Angom, "Relativistic coupled-cluster calculations of ^{20}Ne, ^{40}Ar, ^{84}Kr, and ^{129}Xe: Correlation energies and dipole polarizabilities," Phys. Rev. A **80**, 062505 (2009).

[40] B. K. Mani and D. Angom, "Atomic properties calculated by relativistic coupled-cluster theory without truncation: Hyperfine constants of Mg^+, Ca^+, Sr^+, and Ba^+," Phys. Rev. A **81**, 042514 (2010).

[41] S. Chattopadhyay, B. K. Mani, and D. Angom, "Perturbed coupled-cluster theory to calculate dipole polarizabilities of closed-shell systems: Application to Ar, Kr, Xe, and Rn," Phys. Rev. A **86**, 062508 (2012).

[42] Péter Pulay, "Convergence acceleration of iterative sequences. the case of scf iteration," Chem. Phys. Lett. **73**, 393 – 398 (1980).

[43] Stephan Fritzsche, Brajesh K. Mani, and Dilip Angom, "Chapter 10 A Computer-Algebraic Approach to the Derivation of Feynman-Goldstone Perturbation Expansions for Open-Shell Atoms and Molecules," Advances in Quantum Chemistry **53**, 177–215 (2008).

[44] I. Lindgren and J. Morrison, *Atomic Many-Body Theory* (Springer, Berlin, 2nd Edition, 1986).

[45] P. Jönsson, G. Gaigalas, J. Bieroń, C. Froese Fischer, and I. P. Grant, "New version: Grasp2k relativistic atomic structure package," Comp. Phys. Comm. **184**, 2197 – 2203 (2013).

[46] I P Grant and B J McKenzie, "The transverse electron-electron interaction in atomic structure calculations," J. Phys. B **13**, 2671 (1980).

[47] E. A. Uehling, "Polarization effects in the positron theory," Phys. Rev. **48**, 55–63 (1935).

[48] L. Wayne Fullerton and G. A. Rinker, "Accurate and efficient methods for the evaluation of vacuum-polarization potentials of order $z\alpha$ and $z\alpha^2$," Phys. Rev. A **13**, 1283–1287 (1976).

[49] V. M. Shabaev, I. I. Tupitsyn, and V. A. Yerokhin, "Model operator approach to the lamb shift calculations in relativistic many-electron atoms," Phys. Rev. A **88**, 012513 (2013).

[50] V.M. Shabaev, I.I. Tupitsyn, and V.A. Yerokhin, "Qedmod: Fortran program for calculating the model lamb-shift operator," Computer Physics Communications **189**, 175–181 (2015).

[51] Ian Grant, "Relativistic atomic structure," in *Springer Handbook of Atomic, Molecular, and Optical Physics*, edited by Gordon Drake (Springer, New York, 2006) pp. 325–357.

[52] "Nist atomic spectroscopic database," https://physics.nist.gov/PhysRefData/ASD/levels_for (2013).

[53] M. S. Safronova, U. I. Safronova, and S. G. Porsev, "Polarizabilities, Stark shifts, and lifetimes of the In atom," Phys. Rev. A **87**, 032513 (2013).

[54] S. Chattopadhyay, B. K. Mani, and D. Angom, "Electric dipole polarizability of alkaline-earth-metal atoms from perturbed relativistic coupled-cluster theory with triples," Phys. Rev. A **89**, 022506 (2014).